Development/Plasticity/Repair

Ca_v2.2 Channels Sustain Vesicle Recruitment at a Mature Glutamatergic Synapse

Magdalena Wender,* Grit Bornschein,* Simone Brachtendorf, Stefan Hallermann, Jens Eilers, and Hartmut Schmidt

Carl Ludwig Institute for Physiology, Medical Faculty, Leipzig University, 04103 Leipzig, Germany

The composition of voltage-gated Ca^{2+} channel (Ca_v) subtypes that gate action potential (AP)-evoked release changes during the development of mammalian CNS synapses. $Ca_v2.2$ and $Ca_v2.3$ lose their function in gating-evoked release during postnatal synapse maturation. In mature boutons, $Ca_v2.1$ currents provide the almost exclusive trigger for evoked release, and $Ca_v2.3$ currents are required for the induction of presynaptic long-term potentiation. However, the functional significance of $Ca_v2.2$ remained elusive in mature boutons, although they remain present at active zones and continue contributing significantly to presynaptic Ca^{2+} influx. Here, we addressed the functional significance of $Ca_v2.2$ and $Ca_v2.3$ at mature parallel-fiber (PF) to Purkinje neuron synapses of mice of either sex. These synapses are known to exhibit the corresponding developmental Ca_v subtype changes in gating release. We addressed two hypotheses, namely that $Ca_v2.2$ and $Ca_v2.3$ are involved in triggering spontaneous glutamate release and that they are engaged in vesicle recruitment during repetitive evoked release. We found that spontaneous miniature release is Ca^{2+} dependent. However, experiments with Ca_v subtype-specific blockers excluded the spontaneous opening of Ca_vs as the Ca^{2+} source for spontaneous glutamate release. Thus, neither $Ca_v2.2$ nor $Ca_v2.3$ controls spontaneous release from PF boutons. Furthermore, vesicle recruitment during brief bursts of APs was also independent of Ca^{2+} influx through $Ca_v2.2$ and $Ca_v2.3$. However, $Ca_v2.2$, but not $Ca_v2.3$, currents significantly boosted vesicle recruitment during sustained high-frequency synaptic transmission. Thus, in mature PF boutons $Ca_v2.2$ channels are specifically required to sustain synaptic transmission during prolonged neuronal activity.

Key words: calcium channels; facilitation; N-type; parallel fiber; plasticity; vesicle recruitment

---

Significance Statement

At young CNS synapses, action potential-evoked release is gated via three subtypes of voltage-gated Ca^{2+} channels: $Ca_v2.1$, $Ca_v2.2$, and $Ca_v2.3$. During postnatal maturation, $Ca_v2.2$ and $Ca_v2.3$ lose their function in gating evoked release, such that at mature synapses $Ca_v2.1$ provides the almost exclusive source for triggering evoked release. $Ca_v2.3$ currents are required for the induction of presynaptic long-term potentiation. However, the function of the still abundant $Ca_v2.2$ in mature boutons remained largely elusive. Here, we studied mature cerebellar parallel-fiber synapses and found that $Ca_v2.2$ does not control spontaneous release. However, Ca^{2+} influx through $Ca_v2.2$ significantly boosted vesicle recruitment during trains of action potentials. Thus, $Ca_v2.2$ in mature parallel-fiber boutons participate in sustaining synaptic transmission during prolonged activity.

Introduction

At young parallel-fiber (PF) to Purkinje neuron (PN) synapses, action potential (AP)-induced glutamate release is triggered via

Ca^{2+} influx through voltage-gated Ca^{2+} channels (Ca_vs) of the $Ca_v2.1$, $Ca_v2.2$, and $Ca_v2.3$ types (Mintz et al., 1995; Kusch et al., 2018). During cerebellar maturation, $Ca_v2.2$ and $Ca_v2.3$ essentially lose their function in gating release, and influx through $Ca_v2.1$ becomes the almost exclusive trigger of AP-mediated release. However, $Ca_v2.2$ persists at active zones (AZs) of matured PF boutons (Kusch et al., 2018), and $Ca_v2.2$ as well as $Ca_v2.3$ continue contributing to presynaptic Ca^{2+} influx, such that sources and amplitudes of presynaptic Ca^{2+} signals remain similar during maturation (Myoga and Regehr, 2011; Baur et al., 2015; Kusch et al., 2018). This phenomenon of Ca_v subtype switching in the triggering of evoked release during development is not restricted to PF synapses. At various other inhibitory and excitatory synapses, the contribution of $Ca_v2.2$ and $Ca_v2.3$ to triggering evoked release

was found to decline during development (Iwasaki and Takahashi, 1998; Iwasaki et al., 2000; Fedchyshyn and Wang, 2005; Miki et al., 2013; Nakamura et al., 2015; Bornschein et al., 2019). These findings raise the question of the functional significance of Ca$_v$2.2 and Ca$_v$2.3 in matured boutons.

Ca$_v$2.3 has been shown to control the induction of presynaptic long-term potentiation at PF–PN and hippocampal mossy-fiber synapses, while Ca$_v$2.2 was not engaged in this process (Dietrich et al., 2003; Myoga and Regehr, 2011). In addition, at cultured hippocampal synapses stochastic opening of Ca$_v$2.3 in particular played a prominent role in triggering spontaneous vesicle fusion events (Ermolyuk et al., 2013). Hence, while for Ca$_v$2.3 specific functions beyond triggering AP-evoked release were observed, the significance of presynaptic Ca$_v$2.2 in matured boutons remained rather elusive. We therefore tested the hypothesis of whether Ca$_v$2.2 or also Ca$_v$2.3 provides Ca^{2+} entry for controlling (1) spontaneous miniature release and (2) synaptic vesicle recruitment.

The pool of readily releasable vesicles (RRPs) docked to release sites and the number of release sites are rather limited at small CNS synapses (Brémaud et al., 2007; Valera et al., 2012; Schmidt et al., 2013; Miki et al., 2016; Bornschein et al., 2019). During repetitive neuronal activity, the RRP is progressively used up, and synaptic efficacy as well as plasticity critically depend on the recruitment of new vesicles. At facilitating synapses, recruitment can be very rapid and even give rise to a temporary overfilling of the RRP (Valera et al., 2012; Brachtendorf et al., 2015; Miki et al., 2016; Doussau et al., 2017; Neher and Brose, 2018; Schmidt, 2019; Vandael et al., 2020; Silva et al., 2021). Evidence from different synapses suggests that recruitment is reversible and, at least partially, Ca^{2+} dependent (Neher and Sakaba, 2008; Miki et al., 2016; Doussau et al., 2017; Miki et al., 2018; Imig et al., 2020; Kusick et al., 2020; Miki et al., 2020; Vandael et al., 2020; Eshra et al., 2021; Lin et al., 2022) The specific Ca^{2+} sources involved in regulating recruitment, however, have remained unclear to date (for review, see Schmidt, 2019; Silva et al., 2021).

PF synapses are among the synapses that show rapid vesicle recruitment, which gives rise to their characteristic sustained high-frequency facilitation (Miki et al., 2016; Doussau et al., 2017). They are, therefore, ideally suited to investigate the mechanisms of Ca^{2+}-dependent vesicle recruitment. Furthermore, PFs provide the majority of excitatory inputs to PNs, which makes them also well suitable for studying spontaneous glutamate release. We found that spontaneous release was not reduced by blocking Ca$_v$2 channels with subtype-specific toxins. On the other hand, block of Ca$_v$2.2 but not Ca$_v$2.3 significantly reduced the rate of vesicle recruitment during trains of APs. Hence, our results reveal a significant function of Ca$_v$2.2 in maintaining steady-state recruitment of vesicles during periods of heavy synaptic use.

Materials and Methods

Slice preparation and electrophysiology

Slices were prepared and patch-clamp recordings were performed as described previously (Baur et al., 2015). Briefly, postnatal day 21 (P21) to P24 C57BL/6J mice of either sex were decapitated under deep inhalation anesthesia with isoflurane (CuraMed). The vermis region of the cerebellum was rapidly excised and transferred to cooled (0–4°C) artificial CSF (ACSF) containing the following (in mM): 125 NaCl, 2.5 KCl, 1.25 NaH$_2$PO$_4$, 26 NaHCO$_3$,1 MgCl$_2$, 2 CaCl$_2$, and 20 glucose, equilibrated with 95% O$_2$ and 5% CO$_2$, at pH 7.3–7.4. Parasagittal (electrophysiology) slices (250 μm thick) were cut with a vibratome (Microm HM 650 V) and incubated at 35°C in ACSF for 30 min.
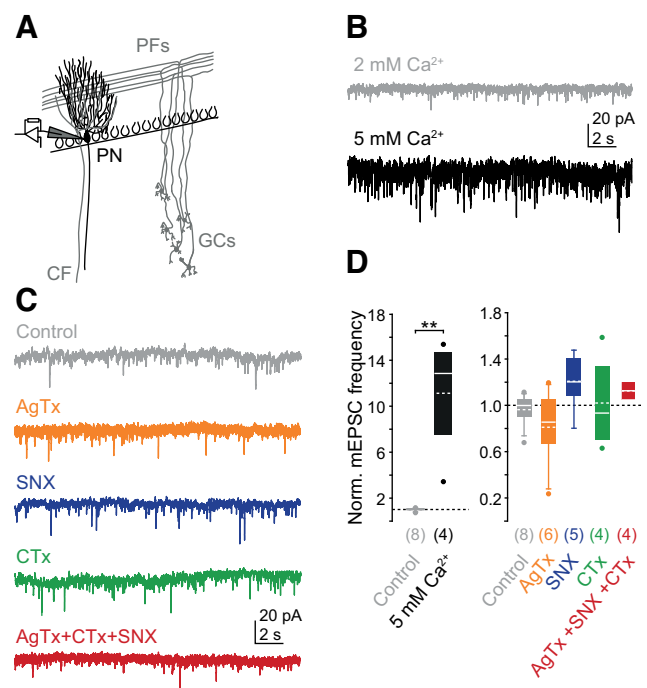
Figure 1. Spontaneous mEPSCs are Ca^{2+} dependent but unaffected by specific Ca$_v$ blockers. **A**, Recording scheme: mEPSCs were recorded from whole-cell patch-clamped PNs in acute brain slices from P21 to P24 mice. Presynaptic sources are mainly granule cells (GCs), particularly via PFs and also the climbing fiber (CF). **B**, Example traces of spontaneous mEPSCs recorded in [Ca^{2+}]$_e$ of 2 mM (standard ACSF, gray, top) or 5 mM (black, middle). Note the increase of spontaneous events in elevated [Ca^{2+}]$_e$. **C**, As in **B** for control conditions (standard ACSF, gray) and after application of AgTx (250 nM; orange), SNX (500 nM; blue), CTx (5 μM; green), or the combination of the three toxins (red). **D**, Summary of averaged mEPSC frequencies after application of high extracellular Ca^{2+} (**p = 0.004), AgTx, SNX, CTx, or all toxins combined (color code as in **B** and **C**). Data were normalized to the averaged mEPSC frequency under control conditions for each specific cell. Note that neither the individual subtype-specific blockers nor their combination significantly affected the mEPSC frequency.

Afterward, slices were stored at room temperature (RT; ∼22°C). For experiments, slices were transferred to a recording chamber that was constantly perfused with 4 ml of ACSF/min supplemented with 10 μM bicuculline (Tocris Bioscience) at RT. Unless stated otherwise, chemicals were from Sigma-Aldrich.

Patch pipettes with a resistance of ∼5 MΩ were prepared with a PC-10 puller (Narishige) from borosilicate glass (Hilgenberg) and filled with the following pipette solution (in mM): 157 K-gluconate, 4 NaCl, 3 MgCl$_2$, 3 Na$_2$-ATP, 0.3 Na-GTP, 0.05 EGTA, and 10 HEPES, dissolved in purified water, with pH adjusted to 7.3 with KOH or HCl.

Whole-cell patch-clamp recordings from PNs were performed under optical control (model BX51WI, Olympus) using an EPC10/3 amplifier and PatchMaster software (version v2x90.2; HEKA). EPSCs were typically recorded at a holding potential of −80 mV corrected for the liquid junction potential (16 mV). Data were filtered at 2–5 kHz and sampled at 10 kHz. Series resistance (R$_s$) and holding current (I$_{hold}$) were monitored continuously. R$_s$ was compensated constantly to a target value of 10 MΩ. Experiments were rejected if the uncompensated R$_s$ exceeded 30 MΩ or if I$_{hold}$ fell below −500 pA. mEPSCs (Fig. 1) were recorded in the presence of 1 μM tetrodotoxin (TTX) added to the bath solution. Baseline recordings and recordings with pharmacological treatments had a duration of 800 s each (40 traces of 20 s).

To evoke EPSCs, PFs were stimulated extracellularly by placing a stimulation pipette containing ACSF in the molecular layer (Fig. 2). Stimulus intensities were adjusted to reach initial evoked EPSC amplitudes of ∼500 pA [interquartile range (IQR) 366–630 pA], using an
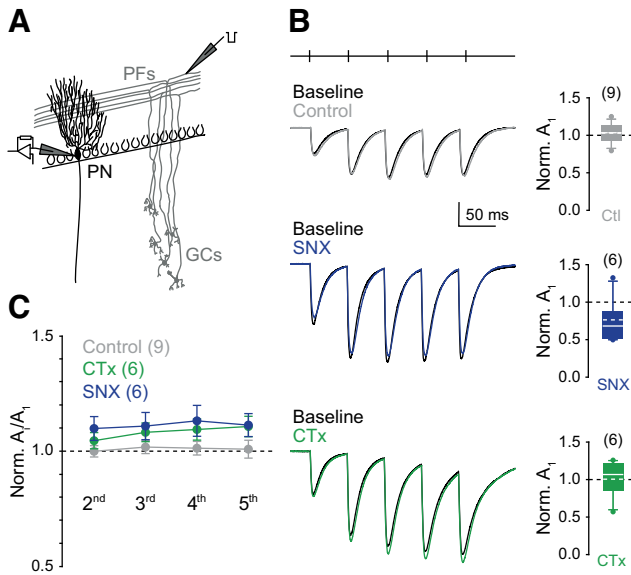
Figure 2. Neither Ca$_v$2.2 nor Ca$_v$2.3 channels affect first EPSC amplitudes and facilitation. **A**, PFs were stimulated extracellularly and evoked EPSCs were recorded from whole-cell patch-clamped PNs. **B**, Left, Examples of EPSCs (average of 10 repeats each) evoked by five stimuli at 20 Hz (top) during baseline recordings (black), control recordings (gray), and after application of SNX (blue) or CTx (green). Stimulation artifacts were removed for clarity. Right, Relative A$_1$ values after mock application of ASCF (control, gray, top) and after the application of SNX (blue, middle) or CTx (green, bottom) normalized to baseline A$_1$ in ACSF. **C**, Averaged A$_i$/A$_1$ ratios (ratio of 2nd, 3rd, 4th, or 5th to 1st EPSCs, respectively) show no effect of SNX (blue) or CTx (green) on facilitation compared with A$_i$/A$_1$ ratios of untreated control recordings. Data are normalized to baseline ratios.

isolated stimulator (model ISO-Stim 01 DPI, NPI Electronics). Using the quantal release parameters of PF synapses ($q = 8\,pA$, $N = 2.9$; Schmidt et al., 2013; Baur et al., 2015) and a vesicular release probability (p_v) of either 0.25 or 0.6 for standard (2 mM) or elevated (6 mM) [Ca^{2+}]$_e$, respectively, we estimate that 86 PFs (range, 63–108) or 36 PFs (range, 26–45) were stimulated on average in these experiments.

Bursts of five stimuli at 20 Hz were applied every 20 s. Following 10 stable baseline recordings, ACSF (mock treatment) or ACSF supplemented with a Ca$_v$ blocker were washed in for 10 min. Subsequently, the effects were quantified from 10 recordings during the treatment. Ca$_v$s were blocked by either 250 nM ω-agatoxin-IVA (AgTx; PEPTIDE), 5 μM ω-conotoxin GVIA (CTx; Bachem), 500 nM SNX-482 (SNX; PEPTIDE), or a combination of the three toxins.

For cumulative analysis (Schneggenburger et al., 1999), the CaCl$_2$ concentration of the ACSF was raised to 6 mM and MgCl$_2$ was omitted to keep the concentration of divalent cations closer to the initial value. Fifty stimuli were applied to PFs at 20 Hz, followed by 9 stimuli at increasing intervals (70 ms, 100 ms, 200 ms, 300 ms, 500 ms, 1 s, 3 s, 5 s, 10 s) to monitor the recovery of synaptic transmission (see Figs. 6, 7). Cumulative analysis was performed on EPSCs during the 20 Hz train. Recovery of transmission was quantified by fitting double-exponential functions to the time course of pulses given between 0.67 and 20.17 s (pulses 54–59) after the end of the train. This protocol was repeated five times in ACSF (baseline) and following a 10 min washin of one of the above toxin blockers (treatment) dissolved in ACSF. Sixty second breaks were used between the individual runs. The runs for each condition were averaged.

Using trains at higher frequencies in a more physiological [Ca^{2+}]$_e$ of ~2 mM results in lasting facilitation at PF synapses (Doussau et al., 2017), which is not favorable for cumulative analysis. Moreover, higher frequencies result in the buildup of a strong tonic release component (Doussau et al., 2017), which complicates the analysis of the phasic release component, in

particular late in the train. We found that both complications were avoided by using the frequency of 20 Hz and 6 mM [Ca^{2+}]$_e$.

All experiments were conducted in accordance with institutional guidelines for animal experiments, and were approved by the state directorate of Saxony, Germany.

Computer simulations
Simple simulations. For the simple simulations (Fig. 3), it was assumed that p_v remains constant during the train. The number of release sites occupied by a releasable vesicle ($n[i]$) during the ith pulse of a train was calculated as follows:

$$n[i] = n[i-1] - p_v * n[i-1] + r, \tag{1}$$

where r is the recruitment rate (Brachtendorf et al., 2015). Quantal contents were calculated by multiplication of $n[i]$ with a p_v of 0.6 or 0.1 for baseline or reduced p_v conditions, respectively. In simulations mimicking the presence of an additional replenishment pool (RP; Fig. 3B,D,F) extra release sites (Valera et al., 2012) were added for pulses 2–4 in Equation 1.

Full model of Ca^{2+} dynamics, release, and recruitment. Details of the model (see Fig. 7) and the fitting procedure have been described previously (Schmidt et al., 2013; Doussau et al., 2017; Kusch et al., 2018). Briefly, the reaction–diffusion systems were converted to ordinary differential equations (ODEs) and numerically solved using NDSolve or NDSolveValue of Mathematica 13 (Wolfram). Spatial resolution of 2 nm was achieved by placing the ODEs in concentric hemi-shells covering a total radius of 450 nm (Palay and Chan-Palay, 1974; Brenowitz and Regehr, 2007). The model included AP-driven gating schemes of Ca$_v$s generating Ca^{2+} influx, endogenous and exogenous Ca^{2+} buffers, diffusion, an extrusion mechanism, and a release sensor.

Given the absence of data from PF synapses, the presynaptic AP waveform was estimated based on data from the calyx of Held using a half-duration of 0.2 ms, a τ_{rise} of 0.1, and a τ_{decay} of 0.25 ms to gate the Ca$_v$s (Borst and Sakmann, 1998; Meinrenken et al., 2002; Bucurenciu et al., 2010; Ermolyuk et al., 2013). Voltage-dependent gating schemes of the Ca$_v$s were taken from Li et al. (2007), assuming a single-channel conductance of 2.5 pS for all channels (Li et al., 2007; Scimemi and Diamond, 2012; Ermolyuk et al., 2013). The Ca^{2+} equilibrium potential was calculated to be 165 mV for 6 mM [Ca^{2+}]$_e$. Each Ca$_v$ had five closed (C) and one open (O) state. The transition between the first five steps was assumed to be voltage dependent, and the last step voltage independent, as follows:

$$C_o \underset{\beta_1(V)}{\overset{\alpha_1(V)}{\rightleftharpoons}} C_1 \underset{\beta_2(V)}{\overset{\alpha_2(V)}{\rightleftharpoons}} C_2 \underset{\beta_3(V)}{\overset{\alpha_3(V)}{\rightleftharpoons}} C_3 \underset{\beta_4(V)}{\overset{\alpha_4(V)}{\rightleftharpoons}} C_4 \underset{b}{\overset{a}{\rightleftharpoons}} O, \tag{2}$$
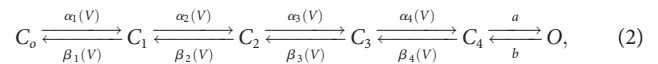
where a and b are the rate constants for transitions between C_4 and O, and $\alpha_i(V)$ and $\beta_i(V)$ are the voltage-dependent forward and backward transition rates that are given by the following:

$$a_i(V) = a_{i,0} \exp(V/k_i), \ i = 1-4, \tag{3}$$

$$\beta_i(V) = b_{i,0} \exp(-V/k_i), \ i = 1-4, \tag{4}$$

where $\alpha_{i,0}$ and $\beta_{i,0}$ are the forward and backward rate constants at 0 mV, and k_i is a slope factor.

Ca^{2+} binding to the binding sites (B) of indicator dyes; of ATP, which acted as a low-affinity, high-capacity endogenous buffer (Sabatini and Regehr, 1998); and of the fifth noncooperative site of calretinin (CR; CR_V) were simulated by second-order kinetics, as follows:

$$\left(\frac{d[Ca^{2+}]}{dt} \right)_j = -k_{\text{on},j}[Ca^{2+}][B_j] + K_{\text{off},j}[Cab_j], \ j = dye, ATP, or\ CR_V. \tag{5}$$

Cooperative Ca^{2+} binding to CR covered tense (T) and relaxed (R) binding sites (Schiffmann et al., 1999; Bastianelli, 2003; Faas et al., 2007), as follows:
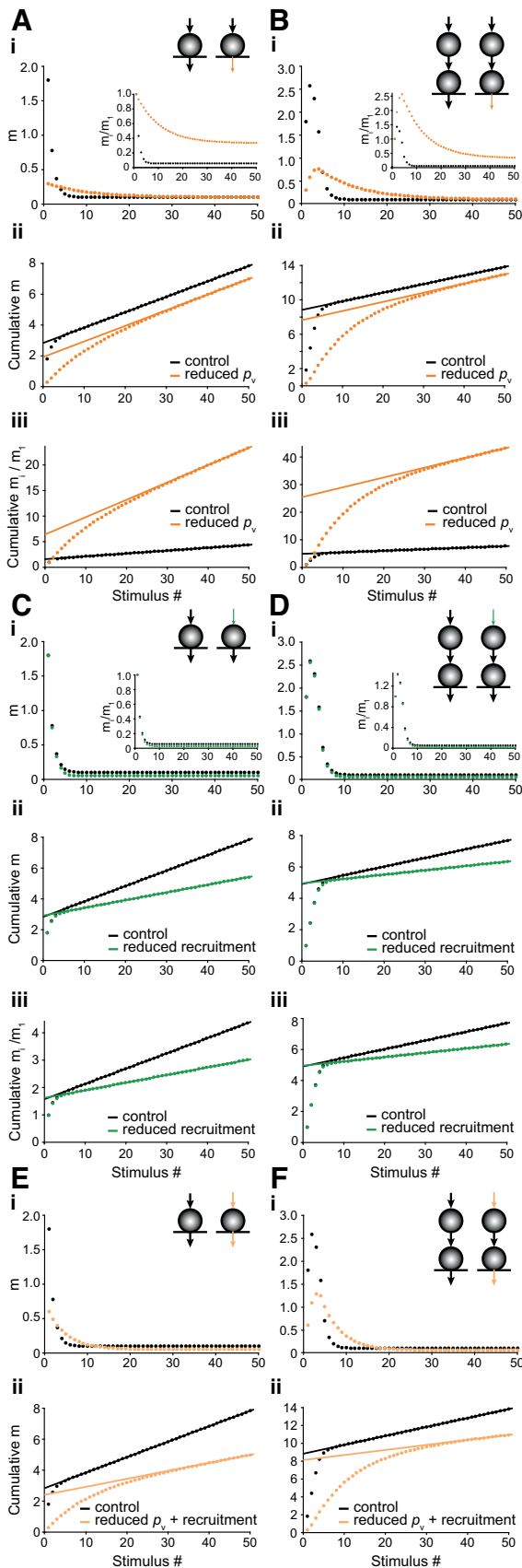
Figure 3. Simple simulations predict treatment-dependent changes for cumulative plots. **Ai**, Top, inset, Scheme of the simulations: release from the RRP ($N = 3$) occurred with high p_v (0.6; control; black) or a reduced p_v (0.1; treatment; orange). Recruitment (black arrow) occurred from an infinite reserve pool (not shown) with rates identical between the two

$$\left(\frac{d[Ca^{2+}]}{dt}\right)_{CRI,II} = -2k_{on,T}[Ca^{2+}][B_{CR1}B_{CRII}] - k_{on,R}[Ca^{2+}][Ca(B_{CR1}B_{CRII})] + 2k_{off.R}[Ca_2(B_{CR1}B_{CRII})] + k_{off.T}[Ca\,(B_{CR1}B_{CRII})].$$

$$\text{(6)}$$

Radial diffusion of each molecular species X was simulated by the following:

$$\left(\frac{d[X]}{dt}\right) = D_X \frac{A_{n,n\pm1}}{V_n r}([X])_{n\pm1} - [X]_n,$$

$$\text{(7)}$$

with D_X being the diffusion coefficient (Bucurenciu et al., 2008; Vyleta and Jonas, 2014), A the surface, V the volume, and r the radius of a shell. Ca^{2+} was cleared by a linear, surface-based extrusion mechanism driven by the difference between $[Ca^{2+}]_i$ and the resting $[Ca^{2+}]_i$ (250 nM assumed for 6 mM $[Ca^{2+}]_e$). Twenty percent of CR was assumed to be immobile (Winsky and Kuźnicki, 1995; Arendt et al., 2013).

For the simulated local or global $[Ca^{2+}]_i$ signals were fit by a Gaussian or double-exponential function and used to drive a five-site model of release with two recruitment steps (Millar et al., 2005; Sakaba, 2008; Doussau et al., 2017). For a description of the release–recruitment model, see Figures 7 and 8 and the corresponding Results section. The simulation only covered Ca$_v$2 in the AZ, according to electron microscopy (EM) particle counts and further estimates derived by Kusch et al. (2018). Local Ca^{2+} at the release sensor resulted from influx through a single Ca$_v$2.1 at a distance of 10 nm to the release sensor and two more remote Ca$_v$2.2. The distance of the Ca$_v$2.2 channels was varied to optimize the overlap between simulation and experimental data. This optimization procedure gave a distance estimate of 24 nm. A simulation with five Ca$_v$2.2 at a distance of 40 nm (Kusch et al., 2018) yielded similar results. Global residual Ca^{2+} was simulated as influx through all Ca$_v$2.1 (six on average) and Ca$_v$2.2 (two on average) in the AZ (Kusch et al., 2018). The residual Ca^{2+} was used to drive recruitment.

←

simulations. For a treatment with such an effect (orange), this simulation predicts an initially reduced m and a slowed drop to a very slightly increased steady-state quantal content. Bottom inset, Simulation following normalization to the first quantal content (m_i/m_1). **Aii**, Cumulative m plots for the simulations shown in **Ai**. Lines were fitted to the steady-state phases and extrapolated to the y-intercepts. For this simulation with reduced p_v (orange), a decreased y-intercept and a very slightly increased slope (black, $2.933 + 0.100\times$; orange, $2.024 + 0.101\times$) are predicted compared with the control (black). **Aiii**, Cumulative plot following normalization to the first quantal content (m_i/m_1). Note that due to the normalization an increased y-intercept is predicted for the simulation with reduced p_v (orange). Furthermore, the normalization amplified the effect of reduced p_v on the slope of the line fit (black, $1.630 + 0.056\times$; orange, $6.750 + 0.340\times$). **B**, As in **A**, but in these simulations an exhaustible replenishment pool was placed between the infinite reserve pool (data not shown) and the RRP. **Bi**, Note that these simulations predict an initial facilitation even for high p_v. **Bi,ii**, They further predict a very slight increase in the steady-state quantal contents (**Bi**), a reduced y-intercept, and a slightly increased slope (black, $8.933 + 0.100\times$; orange, $7.750 + 0.106\times$) in the cumulative plots (**Bii**). **Biii**, The treatment-specific predictions for the normalized cumulative plots are qualitatively identical to those in **A**, but the y-intercept and the slope are further increased (note the differences in ordinate scaling; black, $4.960 + 0.056\times$; orange, $25.830 + 0.350\times$). **C**, As in **A**, but in these simulations p_v was kept constant, while the recruitment rate was reduced (green). **Ci–iii**, For such a treatment, the simulations predict a reduced steady-state amplitude (**i**) and a decline in the slope of the fitted line, while the y-intercept will remain almost unchanged [green, $2.967 + 0.050\times$ (**ii**); $1.650 + 0.028\times$ (**iii**)]. **D**, As in **C**, but in these simulations the exhaustible replenishment pool was introduced as in **B**. **Di–iii**, Again an initial facilitation is predicted (**i**), while for the cumulative plots the predictions remain qualitatively identical to **C** i.e. reduced slope and unchanged y-intercept [green, $8.967 + 0.050\times$ (**ii**); $4.980 + 0.028\times$ (**iii**)]. **Ei,ii**, As in **Ai**, **ii**, but in these simulations p_v and recruitment rate were reduced (light orange). For a pharmacological treatment with both effects, a decrease in slope and y-intercept is predicted (light orange, $2.780 + 0.050\times$). **Fi,ii**, As in **Ei,ii**, but again the exhaustible replenishment pool was introduced as in **B** and **D**. Similar to the simulations in **B** and **D**, an initial facilitation is predicted (**i**) and predictions for the cumulative plots remain qualitatively identical to **E** (light orange, $8.797 + 0.050\times$).

Table 1. Additional model parameters

Parameter		Value		References/remark
Calretinin				Faas et al. (2007)
	Binding sites	5	n	
	$k_{on, \ tense}$	1.8	µM/s	
	$k_{on, \ relaxed}$	310	µM/s	
	$k_{on, \ V}$	7.3	µM/s	
	$k_{off, \ tense}$	53	s	
	$k_{off, \ relaxed}$	20	s	
	$k_{off, \ V}$	252	s	
	Concentration	80	µM	1
	Wash-out corr.	70%		2
	D_{CR}	20	µM²/s	3
ATP				Meinrenken et al. (2002)
	Binding sites	1		
	k_{on}	500	µM/s	
	k_{off}	100,000	s	
	Concentration	540	µM	4
	D_{ATP}	220	µM²/s	5
Fluo-5F				Thermo Fisher Scientific
	Binding sites	1		
	k_{on}	30	µM/s	Scott and Rusakov (2006)
	K_D	1.44	µM	Calibration in pipette solution
	Concentration	140	µM	70% of pipette concentration
	D_{Fluo}	15	µM²/s	6
OGB-5N				Thermo Fisher Scientific
	Binding sites	1		
	k_{on}	2500	µM/s	Faas et al. (2007)
	K_D	24	µM	Delvendahl et al. (2015)
	Concentration	140	µM	70% of pipette concentration
	D_{Fluo}	15	µM²/s	6
D_{Ca}		220	µM²/s	Allbritton et al. (1992)
Ca$_v$2.1				Li et al. (2007)
	a, b	247.71, 8.28	ms	
	$\alpha_{1,0}, \beta_{1,0}$	5.89, 14.99	ms	
	$\alpha_{2,0}, \beta_{2,0}$	9.21, 6.63	ms	
	$\alpha_{3,0}, \beta_{3,0}$	5.2, 132.8	ms	
	$\alpha_{4,0}, \beta_{4,0}$	1823.18, 248.58	ms	
	k1	62.61	mV	
	k2	33.92	mV	
	k3	135.08	mV	
	k4	20.86	mV	
Ca$_v$2.2				
	a, b	615.01, 7.68	ms	
	$\alpha_{1,0}, \beta_{1,0}$	4.29, 5.23	ms	
	$\alpha_{2,0}, \beta_{2,0}$	5.24, 6.63	ms	
	$\alpha_{3,0}, \beta_{3,0}$	4.98, 73.89	ms	
	$\alpha_{4,0}, \beta_{4,0}$	772.63, 692.18	ms	
	k1	68.75	mV	
	k2	39.53	mV	
	k3	281.62	mV	
	k4	18.46	mV	
Ca$_v$2.3				
	a, b	228.83, 1.78	ms	
	$\alpha_{1,0}, \beta_{1,0}$	9911.36, 0.62	ms	
	$\alpha_{2,0}, \beta_{2,0}$	4.88, 21.91	ms	
	$\alpha_{3,0}, \beta_{3,0}$	4.00, 51.30	ms	
	$\alpha_{4,0}, \beta_{4,0}$	256.41, 116.97	ms	
	k1	67.75	mV	
	k2	50.94	mV	
	k3	173.29	mV	
	k4	16.92	mV	
Release sensor				Sakaba (2008)
	Binding sites	5		
	k_{on}	90	µM/s	
	k_{off}	3000	s	

(*Table continues.*)

Table 1. Continued

Parameter		Value		References/remark
	γ	5000	s	
	b	0.25		
	k_1	0.42	s	Fit parameter
	$k'_{1,Ca}$	0.237 * RR	µM/s	Fit parameter
	k_2	8.2	s	Fit parameter
	$k_{2,Ca}$	2.7	µM/s	Fit parameter
	k_{1b}	0.06	s	Fit parameter; 7
	k_{2b}	1.35	s	Fit parameter; 7

1, Assuming that CR is the main native buffer (Schiffmann et al., 1999) and that the endogenous buffer capacity is ~60 (Bastianelli, 2003; Brenowitz and Regehr, 2007); 80 µM CR gives κ = 58 (Faas et al., 2007); 20% of CR was immobile in the simulation (Winsky and Kuźnicki, 1995; Arendt et al., 2013); 2, assuming that CR has a similar time course as dye washin; 3, Value for the related protein Calbindin-D28k (Schmidt et al., 2005; Arendt et al., 2013); 4, calculated free ATP concentration in pipette solution; K = 2.7; 5, assumed to be similar to D_{Ca} (Bucurenciu et al., 2008; Vyleta and Jonas, 2014); 6, assumed to be similar to Oregon Green 488 BAPTA-1 (Schmidt et al., 2003); 7, calculated to stabilize the model with resting [Ca^{2+}]$_i$.

Paired-pulse ratios (PPRs) during train and recovery were calculated as ratios of p_vs or peak release rates to the first p_v or first peak in the train, respectively. No differences were observed between ratios derived by the two different methods (see Fig. 8Cii, exception case). p_vs were derived by temporal integration of the release rates. To prevent overfilling of the initial RRP, Ca^{2+}-independent recruitment started with the onset of release. To correctly predict the sag before recovery from steady state, we had to include an exponentially increasing and subsequently decreasing (τ = 100 ms) value for k_{2b}.

Inclusion of an intrinsic facilitation mechanism that decreased k_{off} 10-fold during the train followed by a return to its initial value after the train would also predict the sag (see Fig. 8Ci), albeit not as prominent as observed experimentally. The simulations with decreasing k_{off} predict that the release time course broadens during the train, which should give rise to a broadening of the EPSCs during the train (see Fig. 8Cii). To probe for EPSC broadening, we compared the experimental A_i/A_1 EPSC ratios (ith EPSC amplitudes/first EPSC amplitude) to their temporal integrals (Q_i/Q_1) during the train. We found that they were almost identical and significantly deviated from each other only between the seventh and ninth pulses in the train [i = 7, p = 0.021; i = 8, p = 0.031; i = 9, p = 0.025; Mann–Whitney U (MWU) test; see Fig. 8Ciii]. This argues against significant EPSC broadening during the train and in turn indicates that intrinsic regulation of k_{off} is unlikely to be a prominent factor in facilitation at PF synapses. Hence, we did not further consider intrinsic facilitation in the simulations. During recovery, the Ca^{2+}-independent rate constants (k_1, k_2) were assumed to exponentially decline (τ_1 = 10 s, τ_2 = 5 s) with progressive filling of the RRP. Model parameters are given in Table 1.

Analysis and statistics

Data were analyzed with custom-written routines in Igor Pro 8 (WaveMetrics). For the analysis of mEPSCs, the macro toolkit Neuromatic (Rothman and Silver, 2018) was used. The automatic detection threshold was set to the highest rms noise value obtained for a given cell and, if necessary, manually adjusted after visual inspection to increase detection accuracy.

Data are presented as the mean ± SEM or the median and 25th to 75th percentile. In box-and-whisker plots, boxes and solid lines represent medians and IQRs, dashed lines represent means, and whiskers represent the 10th and 90th percentiles. Data outside the range of the percentiles are shown as outliers. The number of experiments is indicated in brackets. All other plots show mean values, and whiskers represent SEMs.

For normally distributed samples (Shapiro–Wilk normality test), ANOVA (for more than two groups) was used. Not normally distributed data and small samples were compared with the Mann-Whitney-U (MWU) rank-sum test or ANOVA on ranks (for more than two groups). To compare pretreatment and post-treatment data, the paired t test was used for normally distributed samples and the Wilcoxon signed-rank (WSR) test for not normally distributed and small samples. Statistical

significance is indicated as $*p < 0.05$, $**p < 0.01$, or $***p < 0.001$. Statistical tests were performed with SigmaPlot 11.0 (Dundas Software).

Data availability
The Mathematica code is available via a link to github on our homepage (https://physiologie.medizin.uni-leipzig.de/?en,id140) or directly at github (https://github.com/Hartmut-Schmidt/JNeurosci_2023).

Results

Spontaneous release is independent of Ca^{2+} influx through Ca$_v$s

To analyze the function of Ca$_v$s in mature PF boutons, we started by investigating AP-independent, spontaneous miniature EPSCs (mEPSCs). PNs in acute cerebellar slices from matured mice (P21 to P24) were whole-cell patch clamped, and mEPSCs were recorded in the presence of TTX (1 μM) and bicuculline (10 μM; Fig. 1A).

First, we investigated the Ca^{2+} dependency of spontaneous release by varying the extracellular Ca^{2+} concentrations ([Ca^{2+}]$_e$). An increase in [Ca^{2+}]$_e$ from 2 to 5 mM resulted in a significant increase in the frequency of mEPSCs by a factor of 12.85 (range, 5.18–15.05; $n = 4$; control: 1.00; range, 0.89–1.06; $n = 8$; $p = 0.004$, MWU rank-sum test; Fig. 1B,D). The mEPSC amplitudes, on the other hand, showed only a small and insignificant increase in high [Ca^{2+}]$_e$ (factor of 1.20; range, 0.99–1.34; $n = 4$; control: 0.99; 0.96–1.01; $n = 8$; $p = 0.214$, MWU rank-sum test; data not shown). These findings are consistent with findings from different synapses (for review, see Smith et al., 2012; Williams and Smith, 2018), including previous reports about the Ca^{2+} dependency of spontaneous glutamate release onto PNs (Yamasaki et al., 2006; Groffen et al., 2010).

One potential mechanism that could explain an effect of [Ca^{2+}]$_e$ on the frequency of mEPSCs is the stochastic opening of Ca$_v$2 channels, forming transient presynaptic Ca^{2+} microdomains (Ermolyuk et al., 2013). Previous results from several glutamatergic synapses showed that the unspecific inorganic Ca$_v$ blocker Cd^{2+} did not reduce or even increased spontaneous release (Abenavoli et al., 2002; Vyleta and Smith, 2011; Williams and Smith, 2018). In particular, Cd^{2+} was described previously as being ineffective in interfering with spontaneous glutamate release onto PNs (Yamasaki et al., 2006). However, the application of Ca$_v$2 subtype-specific toxins resulted in a significant reduction of the frequency of glutamatergic minis in cultured hippocampal neurons (Ermolyuk et al., 2013). Therefore, we recorded mEPSCs in the presence of AgTx (250 nM), SNX (500 nM), and CTx (5 μM; Fig. 1C,D) that specifically block Ca$_v$2.1, Ca$_v$2.2, and Ca$_v$2.3 channels, respectively. For Ca$_v$2.3, the block could be incomplete because of a fraction of SNX-insensitive channels (Newcomb et al., 1998; Myoga and Regehr, 2011). We quantified the effects of the three toxins as treatment/pretreatment baseline ratios. This analysis revealed that none of the three toxin blockers or their combination had a significant effect on the frequency of mEPSCs (CTx: 0.93; range, 0.67–1.46; $n = 4$; SNX: 1.20; range, 0.99–1.43; $n = 5$; AgTx: 0.86; 0.56–1.09; $n = 6$; all toxins combined: 1.13; 1.05–1.19; $n = 4$; $p = 0.110$, ANOVA on ranks). Also, the corresponding ratios of the amplitudes remained unaffected by application of the toxins (CTx: 1.00; range, 0.94–1.02; $n = 4$; SNX: 1.03; range, 1.01–1.06; $n = 5$; AgTx: 0.95; 0.90–1.04; $n = 6$; $p = 0.098$, ANOVA on ranks; data not shown). Thus, the use of Ca$_v$2 subtype-specific toxins did not reveal a contribution of these channels to miniature glutamate release from PF boutons.

Together, results obtained with specific Ca$_v$2 blockers suggest that spontaneous glutamate release from PF boutons is independent of the opening of Ca$_v$2 channels, although it was dependent on extracellular Ca^{2+}. We consider it unlikely that problems with handling of the blockers are responsible for this result since in our hands the application of the toxins significantly affected presynaptic [Ca^{2+}]$_i$ signals and evoked EPSCs (Kusch et al., 2018). The conclusion is based on the effects of specific Ca$_v$2 subtype-specific toxins rather than the effects of block by Cd^{2+}, thereby avoiding potential occlusion of Cd^{2+}-induced block of Ca$_v$2 by unspecific effects of Cd^{2+} that tended to increase spontaneous release at previously investigated glutamatergic synapses (Vyleta and Smith, 2011; Williams and Smith, 2018).

Neither Ca$_v$2.2 nor Ca$_v$2.3 drive overfilling of the RRP during brief bursting activity

To test whether Ca$_v$2.2 and Ca$_v$2.3 channels contribute to vesicle recruitment and overfilling, we first investigated facilitation during brief bursts of APs evoked by five stimuli at 20 Hz applied to PFs (Fig. 2A,B). Evoked EPSCs recorded from the postsynaptic PN were normalized to the first amplitude (A$_i$/A$_1$, $i = 2$–5), resulting in four PPRs. It was previously shown that neither Ca$_v$2.2 nor Ca$_v$2.3 channels influence the initial p_v and A$_1$ at matured PF–PN synapses (Kusch et al., 2018). Hence, if Ca$_v$2.2 or Ca$_v$2.3 were to be involved in vesicle recruitment, we would expect that pharmacologically blocking these channels would reduce facilitation.

We confirm that blocking of Ca$_v$2.3 and Ca$_v$2.2 channels by SNX or CTx, respectively, had no effect on A$_1$ (normalized to baseline; SNX: 0.76 ± 0.13, $n = 6$; CTx: 1.01 ± 0.11, $n = 6$; control: 1.03 ± 0.05, $n = 9$; $p = 0.102$, one-way ANOVA; Fig. 2B). However, short-term plasticity also was not significantly affected by the application of SNX (A$_i$/A$_1$ for $i = 2$–5: 1.10 ± 0.05, 1.11 ± 0.06, 1.13 ± 0.07, 1.11 ± 0.05; $n = 6$) or application of CTx (A$_i$/A$_1$ for $i = 2$–5: 1.05 ± 0.04, 1.08 ± 0.04, 1.09 ± 0.05, 1.11 ± 0.04; $n = 6$) compared with the control (A$_i$/A$_1$ for $i = 2$–5: 1.00 ± 0.02, 1.02 ± 0.03, 1.01 ± 0.03, 1.01 ± 0.04; $n = 9$; $p = 0.164$, $p = 0.270$, $p = 0.175$, $p = 0.165$, one-way ANOVA; Fig. 2C). Hence, in the absence of significant effects of SNX or CTx on first EPSC amplitudes and facilitation, these findings indicated that Ca$_v$2.2 and Ca$_v$2.3 channels do not play a crucial role for rapid recruitment and overfilling during brief bursts of APs at PF–PN synapses.

Ca$_v$2.2 channels increase the rate of vesicle recruitment during sustained high-frequency activity

We proceeded by investigating steady-state vesicle recruitment during sustained high-frequency synaptic activity. First, we used two simple models of vesicle pools, release and recruitment, to theoretically explore how cumulative quantal contents (m) would be affected by three different cases of pharmacological treatments that would affect only p_v, only the recruitment rate, or both (Fig. 3). The first model contained an RRP and a reserve pool (Fig. 3A,C,E), and the second model contained an additional exhaustible RP intercalated between the RRP and reserve pool (Fig. 3B,D, F). During a train, the first model immediately showed depression (Fig. 3Ai,Ci,Ei), while the second model showed initial facilitation followed by depression later in the train (Fig. 3Bi,Di, Fi). The slopes of linear fits to the late phases of the cumulative plots provide estimates of the steady-state recruitment rates and their back-extrapolated y-intercepts yield a quantity close to the decrement of the RRP during the train (Schneggenburger

et al., 1999; Neher, 2015). Irrespective of the model details, the simple simulations predict that a treatment that reduces p_v without concomitantly affecting the recruitment rate will reduce the y-intercept because of the reduced consumption of releasable vesicles (Fig. 3Aii, Bii). The simulations further predict a very slight increase in the steady-state quantal contents and in the slopes of the line fits in the cumulative plots. On the other hand, a treatment that would only reduce the recruitment rate without concomitantly affecting p_v will result in a shallower slope and essentially no effect on the y-intercept (Fig. 3Cii,Dii). Finally, a treatment that reduces recruitment and p_v will reduce both slope and y-intercept (Fig. 3Eii,Fii).

In the simple simulations, we observed that normalization to the first quantal content (m_1) amplifies specific predictions. In particular, the increased slope during a treatment that only reduces p_v became substantially more pronounced (Fig. 3Aiii,Biii). While the normalization procedure boosts this otherwise very small effect on the slope, it comes at the expense of another, somewhat counterintuitive, prediction. A treatment that only affects p_v is predicted to increase the y-intercept, rather than to decrease it. For a treatment that only reduces the recruitment rate, on the other hand, the normalization does not alter the principle results compared with those obtained with the absolute quantal contents (Fig. 3Ciii,Diii).

To experimentally explore the contributions of the different Ca$_v$2 subtypes to steady-state vesicle recruitment, we applied trains of 50 stimuli at 20 Hz under control conditions and in the presence of AgTx, SNX, or CTx (Fig 4). Trains were repeated five times for each condition and averaged (for details, see Materials and Methods). To achieve a steady-state between release and recruitment (Neher, 2015), these train experiments were performed in 6 mM [Ca^{2+}]$_e$, which will increase p_v to

←

Figure 4. Ca$_v$2.1 and Ca$_v$2.2 channels are significant for steady-state vesicle recruitment. **Ai,** Examples of averaged EPSC trains (n = 5 repetitions each) recorded in 6 mM [Ca^{2+}]$_e$ and at 20 Hz before (black) and after (orange) application of AgTx (250 nM). Inset, Relative 1st (A$_1$) and 50th (A$_{50}$) EPSC amplitudes after application of AgTx normalized to 1st and 50th baseline amplitudes, respectively (*p = 0.031). **Aii,** Cumulative A$_i$ plots (dots) calculated from the EPSCs in **Ai** with back-extrapolated linear fits to the steady-state phases (A$_{40}$ to A$_{50}$). Baseline (black): slope = 3.3 nA/s; y-intercept = 9.0 nA; AgTx (orange):

~0.6–0.7 (Schmidt et al., 2013; Baur et al., 2015). Notably, even with this high p_v, release was facilitated during the initial approximately five APs under control conditions with maximum A_i/A_1 of ~1.25, before gradual depression to a steady state of ~0.3. According to the above simple simulations (Fig. 3), this indicates the presence of a RP (c.f. Miki et al., 2016; Doussau et al., 2017).

We found that EPSC amplitudes during the train were differentially affected by the toxins. As expected (Kusch et al., 2018), the Ca$_v$2.1 blocker AgTx significantly reduced the initial amplitude A_1 relative to the baseline condition (normalized A_1 = 0.26; range, 0.23–0.31; p = 0.031, WSR test). Yet, AgTx did not fully eliminate A_1, which may indicate that in 6 mM [Ca^{2+}]$_e$ more remote Ca$_v$2 subtypes, in particular Ca$_v$2.2 (Kusch et al., 2018), could contribute to triggering evoked release early in the train. The amplitudes late in the train (quantified by A_{50}) were not reduced by AgTx. They were rather slightly albeit not significantly increased compared with the baseline condition (normalized A_{50} = 1.28; range, 0.84–1.69; n = 6; p = 0.844, WSR test; Fig. 4Ai).

The application of SNX had no significant effect on the EPSC amplitudes during the whole train (normalized A_1 = 1.13; range, 0.96–1.38, n = 7; p = 0.375, WSR test; normalized A_{50} = 1.32; range, 0.86–1.68, n = 7; p = 0.813, WSR test; Fig. 4Bi). The application of the Ca$_v$2.2 blocker CTx, on the other hand, slightly reduced A_1 in 6 mM [Ca^{2+}]$_e$ (normalized A_1 = 0.81; range, 0.67–0.98; n = 10; p = 0.049, WSR test). Interestingly, and in contrast to AgTx, CTx also significantly reduced the EPSC amplitudes later in the train. This was again quantified by the effect of CTx on A_{50} (normalized A_{50} = 0.67; range, 0.58–0.73; n = 10; p = 0.006, WSR test; Fig. 4Ci).

To gain more quantitative insights into the differential effects of Ca$_v$2 subtype-specific blockers on sustained release, we performed a cumulative analysis of the train experiments. In this analysis, the slope of the line fits will report differential effects of the toxins on vesicle recruitment rates. The y-intercept, on the other hand, will report the differential effects of the toxins on the decrement of the RRP (multiplied by the number of fibers in tract stimulations) during the train (Neher, 2015). Next to the slope, this decrement is the quantity that could be affected by the toxin treatments, rather than the absolute size of the initial RRP before stimulation. Hence, we analyzed the y-intercepts without correction for incomplete pool depletion (Neher, 2015).

The cumulative analysis revealed that the application of AgTx tended to increase the average slope of the line fits compared with the baseline (baseline, 2.94 ± 0.42 nA/s; AgTx, 3.23 ± 0.59 nA/s; mean ± SEM; n = 6; p = 0.665, paired t test). The y-intercept, on the other hand, was significantly reduced (baseline, 7.40 ± 1.25 nA; AgTx, 4.34 ± 1.07 nA; n = 6; p = 0.015, paired t test; Fig. 4Aii,Aiii). As expected, the application of SNX had no significant effect in the cumulative analysis on either the slopes (baseline, 3.81 ± 0.99 nA/s; SNX, 3.63 ± 0.93 nA/a; n = 7; p = 0.706, paired t test; Fig. 4Bii,Biii) or the y-intercepts (baseline, 8.28 ± 2.72 nA; SNX, 7.10 ± 3.54 nA; n = 7; p = 0.754, paired t test). Unlike AgTx, Ca$_v$2.2 block by CTx resulted in a significant decrease in the slope (baseline, 2.72 ± 0.39 nA/s; CTx, 1.97 ± 0.35 nA/s; n = 10; p = 0.014, paired t test), while leaving the y-intercept statistically unaffected (baseline:,7.04 ± 0.78 nA; CTx, 5.67 ± 0.93 nA; n = 10; p = 0.055, paired t test; Fig. 4Cii,Ciii).

Considering the predictions from the simple models (Fig. 3), these experiments suggest that Ca$_v$2.2 currents are involved in regulating steady-state vesicle recruitment during high-frequency synaptic activation. They argue against an involvement of Ca$_v$2.3 currents in release and recruitment. Ca^{2+}

influx through Ca$_v$2.1 channels, on the other hand, appears as a major regulator of p_v.

Although we aimed at adjusting A_1 to similar values between different cells, the number of activated fibers and synapses will slightly vary between runs and cells during the repeated fiber tract stimulations. Normalization to A_1 provides a means to correct for such variations (Valera et al., 2012; Baur et al., 2015; Doussau et al., 2017). Furthermore, the simple simulations indicated that the normalization could facilitate the detection of the effects of AgTx in the cumulative analysis (Fig. 3Aiii). Hence, we also performed the cumulative analysis on the train data following normalization to A_1 (Fig. 5). The results we obtained from the cumulative analysis of the normalized train data (Figs. 3, 5) are fully in line with the results of the absolute data and reinforce our above conclusions (Figs. 3, 4). In particular, they confirm the function of Ca$_v$2.2 in regulating recruitment and the dominating role of Ca$_v$2.1 in regulating p_v.

Strong block of Ca$_v$2.1 may occlude a potential additional role of these channels in vesicle recruitment because of the very strong reduction of p_v. Hence, to investigate a potential additional function of Ca$_v$2.1 in regulating recruitment, we also performed train experiments with weak block of Ca$_v$2.1 (Fig. 4D). We found that the application of only 100 nM AgTx reduced A_1 to a value similar to that obtained with CTx (normalized A_1 = 0.68; range, 0.41–0.85; n = 8; p = 0.008, WSR test). We further observed that the weak block by AgTx indeed resulted in a significant reduction of the EPSC amplitudes late in the train (normalized A_{50} = 0.69; 0.55–0.73; n = 8; p = 0.008, WSR test; Fig. 4Di). In the cumulative analysis, the y-intercept and the slope were significantly reduced (slope: baseline, 2.78 ± 0.31 nA/s; 100 nM AgTx, 1.77 ± 0.23 nA/s; n = 8; p = 0.001, paired t test; y-intercept: baseline, 7.42 ± 0.70 nA; 100 nM AgTx, 4.85 ± 0.48 nA; n = 8; p = 0.005, paired t test; Fig. 4Dii,iii). These results indicate that Ca$_v$2.1 not only regulates p_v but also contributes to vesicle recruitment (Fig. 3E,F).

Thus, different lines of evidence from data with high-frequency trains of EPSCs in 6 mM [Ca^{2+}]$_e$ indicate that Ca$_v$2.1 channels are the main regulators of p_v and that their current is also significantly involved in regulating steady-state vesicle recruitment. Importantly, the data further indicate Ca$_v$2.2 channels as significant regulators of steady-state vesicle recruitment in addition to Ca$_v$2.1. Ca$_v$2.3 channels, on the other hand, were not involved in the regulation of any of these processes.

Recovery from steady state is independent of Ca^{2+} influx through Ca$_v$2.2 and Ca$_v$2.3 channels

We continued by analyzing the recovery from steady state before and after the application of the three toxin blockers. Following the high-frequency trains, we applied stimuli at increasing intervals (Fig. 6Ai,Ci). In baseline recordings, we observed a characteristic "sag" during the initial stimulations at increasing intervals (i.e., the EPSC amplitudes first declined and only subsequently recovered). The negative peak of this sag occurred ~370 ms after termination of the 20 Hz train. The occurrence of this sag remained unaffected by the application of any of the three toxins (Fig. 6Aii,iii, Cii,iii). This may indicate that a depression mechanism that is independent of Ca$_v$2 channels contributes to the sag.

Following the sag, the time course of recovery could be described by double exponential functions. The double exponential time course remained statistically unaffected by block of Ca$_v$2.3 and Ca$_v$2.2 channels (SNX: τ_{fast} = 1.72 s; range, 0.63–
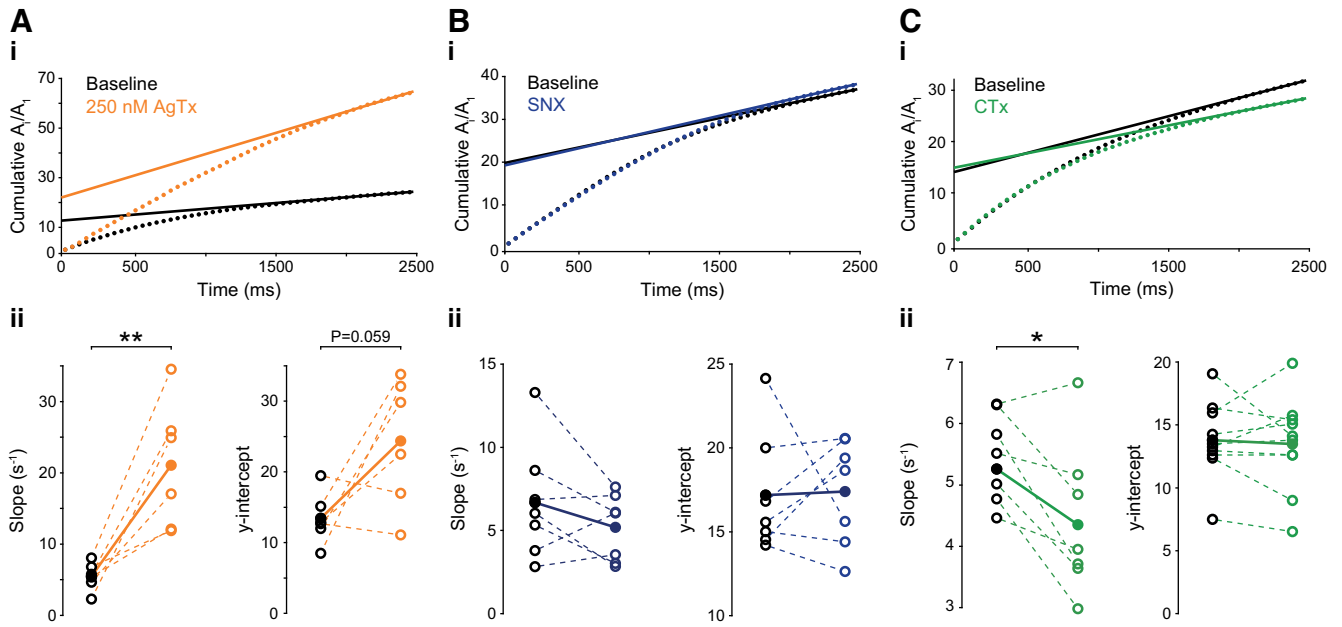
Figure 5. Cumulative analysis on normalized data. ***Ai***, Normalized cumulative A_i/A_1 plots (dots) calculated from the data. Linear fits from A_{40} to A_{50} were back-extrapolated to the y-intercept as in ***Aii***. Baseline (black): slope = 4.6 s^{-1}, y-intercept = 12.9; AgTx (orange): slope = 17.1 s^{-1}, y-intercept = 22.5. ***Aii***, Summary of slopes and y-intercepts before (black) and after (orange) treatment with AgTx. Normalized analysis revealed that the application of AgTx significantly increased the slope (5.5 $\pm$ 0.8 s^{-1}) compared with baseline (21.1 $\pm$ 3.7 s^{-1}; **p = 0.007). It resulted in a twofold increase in the y-intercept that, however, was no longer significant due to the scatter in the normalized data (AgTx, 24.4 $\pm$ 4.5; baseline, 13.4 $\pm$ 1.5; p = 0.059). ***B***, As in ***A***, but for SNX (blue). ***Bi***, Baseline: slope = 6.9 s^{-1}, y-intercept = 20.0; SNX: slope = 7.1 s^{-1}, y-intercept = 20.6. ***Bii***, Data summary. The application of SNX had no significant effect, neither on the slopes (SNX, 5.2 $\pm$ 0.8 s^{-1}; baseline, 6.7 $\pm$ 1.3 s^{-1}) nor on the y-intercepts (SNX, 17.4 $\pm$ 1.2; baseline, 17.2 $\pm$ 1.4). ***C***, As in ***A***, but for CTx (green). ***Ci***, Baseline: slope = 7.1 s^{-1}, y-intercept = 14.3; CTx: slope = 5.4 s^{-1}, y-intercept = 15.1. ***Cii***, Note, that CTx significantly decreased the slope (4.4 $\pm$ 0.4 s^{-1}) compared with baseline (5.3 $\pm$ 0.4 s^{-1}; *p = 0.018), while the y-intercept remained unaffected (CTx, 13.5 $\pm$ 1.2; baseline, 13.8 $\pm$ 1.0).
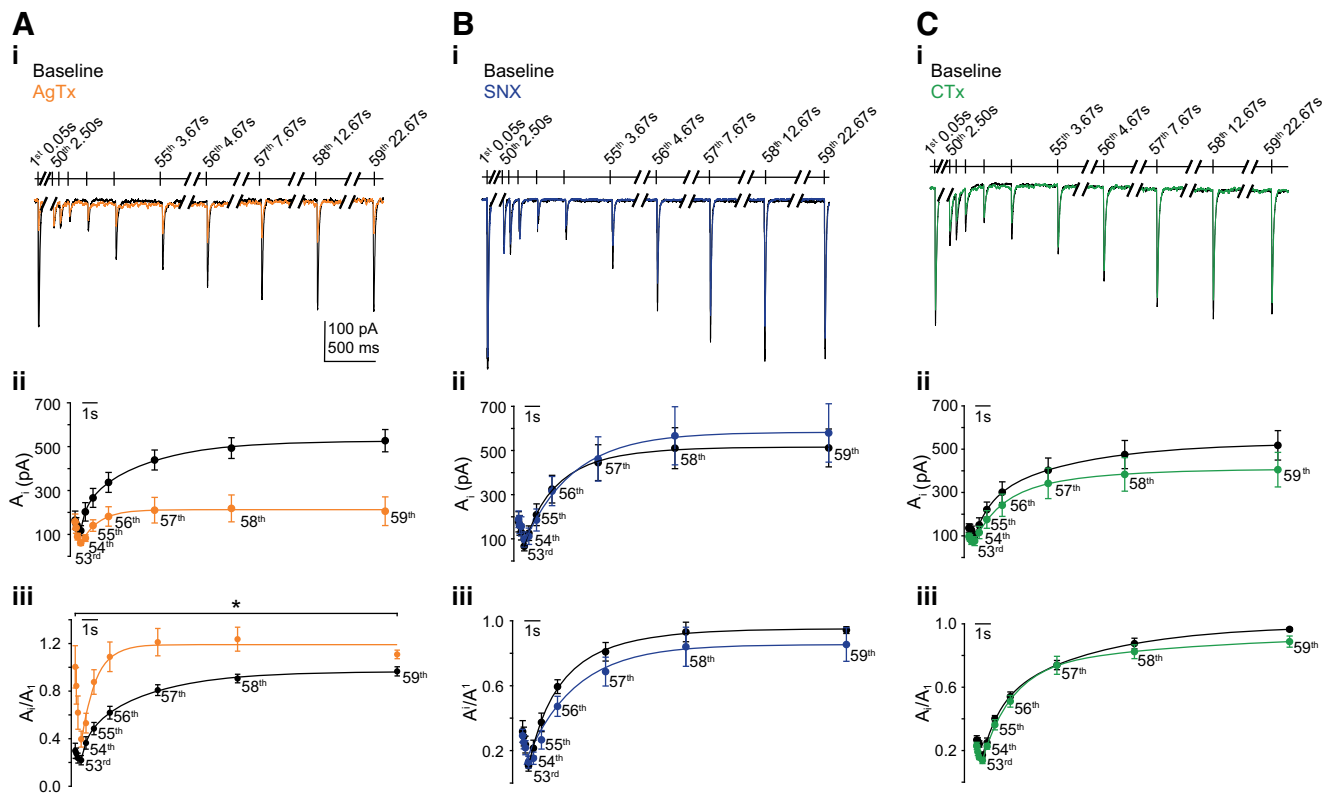
Figure 6. Recovery from steady state is not affected by block of Ca$_V$2.2 and Ca$_V$2.3 channels. ***Ai***, Examples showing the 1st and the 50th EPSC of a 20 Hz train and nine consecutive EPSCs at increasing interstimulus intervals (70 ms, 100 ms, 200 ms, 300 ms, 500 ms, 1 s, 3 s, 5 s, 10 s) to monitor recovery from steady state during the train. Baseline in black, application of AgTx in orange. ***Aii***, Averaged EPSC amplitudes during recovery before (black) and after (orange) the application of AgTx (n = 6 cells). Solid lines represent fits with biexponential functions. ***Aiii***, As in ***ii***, but EPSCs were normalized to the 1st amplitude in the train (A_i/A_1). ***Bi–iii***, As in ***Ai–iii***, but for SNX (blue; n = 7). ***Ci–iii***, As in ***Ai–iii***, but for CTx (green; n = 9).

2.70 s; τ_{slow} = 4.17 s; range, 1.97–25.58 s; n = 7; vs baseline: τ_{fast} = 1.79 s; range 0.99–2.27 s; p = 0.469; τ_{slow} = 2.29 s; range, 1.80–5.51 s; p = 0.297; CTx: τ_{fast} = 0.78 s; range, 0.58–2.11 s; τ_{slow} = 3.54 s; 2.02–11.85 s; n = 9; vs baseline: τ_{fast} = 0.67 s; range, 0.31–2.26 s; p = 0.820; τ_{slow} = 7.42 s; range, 3.54–19.95 s; p = 0.164, WSR test). Strong block of Ca$_v$2.1 by AgTx, on the other hand, significantly accelerated the recovery (AgTx: τ_{fast} = 0.55 s; range, 0.42–0.69 s; τ_{slow} = 0.92 s; range, 0.57–5.15 s; n = 6; vs baseline: τ_{fast} = 1.77 s; range, 1.52–1.98 s; p = 0.031; τ_{slow} = 5.40 s; range, 2.03–24.67 s; p = 0.031, WSR test). However, this significant effect is likely to be a result of the strong reduction of p_v and A$_1$ by the high concentration of AgTx. Strong block by AgTx resulted in the absence of a depression during the steady state. In turn, the recovery measured in the presence of AgTx does not reflect the recovery from a depressed steady state but rather a recovery of transmission from the sag.

Together, the recovery from a depressed steady state was not affected by application of blockers of Ca$_v$2.3 or Ca$_v$2.2 currents. This may indicate the existence of a Ca^{2+}-independent component in the vesicle recruitment pathways.

Models predict Ca^{2+}-dependent and Ca^{2+}-independent recruitment steps

The above data indicated a complex interplay between Ca$_v$2.1 and Ca$_v$2.2, and potentially also Ca^{2+}-independent mechanisms, in regulating release and recruitment processes at PF–PN synapses. The occurrence of a sag before the recovery from steady-state transmission during sustained high-frequency activity adds additional complexity. To gain deeper mechanistic insights into this complexity, we used kinetic spatially resolved reaction–diffusion models of AP-mediated presynaptic Ca^{2+} dynamics, release and recruitment (Figs. 7, 8). For fitting the model to Ca^{2+} signals in PF boutons (Kusch et al., 2018), it contained gating and conductance schemes of Ca$_v$2.1, 2.2, 2.3, ATP, mobile (with whole-cell washout correction) and immobile calretinin, and a Ca^{2+} indicator dye. It was fitted to measured Ca^{2+} signals evoked by bursts of APs, as described previously (Kusch et al., 2018). Subsequently, the model was corrected for the altered driving force in 6 mM [Ca^{2+}]$_e$, and the indicator dye and washout correction were removed. For simplicity, Ca$_v$2.3 channels also were omitted since experimentally we had observed no significant effect of SNX (Fig. 7A). The simulated [Ca^{2+}]$_i$ was used to drive a five-site model of release with two sequential recruitment steps (Millar et al., 2005; Sakaba, 2008). The model included the RP (Fig. 3), which appears as current consent at PF synapses (Miki et al., 2016; Doussau et al., 2017; Neher and Brose, 2018; Miki et al., 2018; Schmidt, 2019). The size of the RP was twofold larger than that of the RRP, and the simulations permitted overfilling of the RRP. The RP was replenished via two pathways, from the recycling of released vesicles (Sakaba, 2008; Doussau et al., 2017) and via an infinite reserve pool (Fig. 7A, middle). We previously found a similar model to be suitable of predicting high-frequency facilitation and low-frequency depression at PF–PN synapses (Doussau et al., 2017).

Considering only Ca$_v$s in the AZ, the release of a vesicle in the RRP was triggered via a local Ca^{2+} signal from a tightly coupled Ca$_v$2.1 channel and two more remote Ca$_v$2.2 channels (Kusch et al., 2018). The simulated p_v in 6 mM [Ca^{2+}]$_e$ under baseline conditions was 0.65, which is in agreement with results from fluctuation analysis (Schmidt et al., 2013; Baur et al., 2015). We focused on the train experiments with strong block by AgTx

and CTx. The block of Ca$_v$2.1 or Ca$_v$2.2 currents reduced the p_v to 0.04 or 0.42, respectively. Thus, to correctly predict the experimental EPSC trains recorded in 6 mM [Ca^{2+}]$_e$, the remote Ca$_v$2.2 channels also contributed to regulating p_v (Fig. 7A; Materials and Methods). This contribution was only present in the elevated [Ca^{2+}]$_e$ as a result of the increased driving force and the strong nonlinearity of the Ca^{2+}-binding curve of the release sensor (Sakaba, 2008).

The rate constants for recruitment to the RP (k_1, k'_1) and the transition from RP to RRP (k_2) could be basal, Ca^{2+} independent or Ca^{2+} dependent, or both. In the simplest version of the model, all rate constants were Ca^{2+} independent. In this form, the model well predicted the A$_i$/A$_1$ during the train under control conditions. However, it failed to reproduce the effects of blocking Ca$_v$2.1 or Ca$_v$2.2 currents (Fig. 8A). Upon making k'_1 Ca^{2+} dependent ($k'_{1,Ca}$), the principal characteristics of the experimental time courses were reproduced by the model (Fig. 8B). Finally, the fit of the model to the complete set of data were improved, if k_2 had a Ca^{2+}-dependent ($k_{2,Ca}$) and a Ca^{2+}-independent component (Fig. 7A,B).

For the Ca^{2+}-dependent rate constants, we assumed that the global [Ca^{2+}]$_i$ from six Ca$_v$2.1 and two Ca$_v$2.2 channels increases the rates, which is the average number of these Ca$_v$s found in freeze fracture replica labeling EM of AZs of PFs (Kusch et al., 2018). The Ca^{2+}-independent components of the constants were required to fit facilitation early in the train. Facilitation in turn had two components, the "active Ca^{2+}" (Katz and Miledi, 1968) remaining bound to the release sensor (Bornschein et al., 2013; Doussau et al., 2017) and, to a much larger degree, overfilling of the RRP (Fig. 7A, right, B, insets; Miki et al., 2016; Doussau et al., 2017). With these settings, the model well predicted the experimental high-frequency EPSC trains (Fig. 7B). It explains their time courses by important contributions of Ca$_v$2.2-dependent and Ca^{2+}-independent mechanisms to recruitment, next to the contribution of Ca$_v$2.1. The model explains the absence of depression during strong block by AgTx late in the train as a result of the strongly reduced p_v and the intact Ca$_v$2.2-dependent and Ca^{2+}-independent recruitment. This results in a lasting overfilling of the RRP and the absence of steady-state depression (Fig. 7Bii). Of note, in the simulations of the toxin experiments all parameters were kept as in the simulations of the controls. Only the corresponding Ca^{2+} currents were blocked in the simulations.

All three time courses of recovery after the 20 Hz trains were also reasonably well predicted by the simulations (Fig. 7C). However, to predict the initial sag before recovery, we had to assume ad hoc a ~500 ms period after the high-frequency train with an exponentially increasing and subsequently decreasing (τ = 100 ms) tendency of vesicles to undock from the RRP toward the RP (i.e., a temporary increase in k_{2b}; Fig. 7A, middle, right). This requirement of a Ca^{2+}-independent mechanism is consistent with the experimental findings that the occurrence of the sag remained unaffected by blocking of Ca$_v$2 channels. Thus, with Ca^{2+}-dependent and Ca^{2+}-independent rate constants and the assumption of an additional Ca^{2+}-independent depression mechanism the model well predicted the complete experimental time courses under control conditions as well as in the presence of the subtype-specific toxin blockers of Ca$_v$2.1 and Ca$_v$2.2 (Fig. 7C). Next to the contribution of Ca$_v$2.1, the model predicts important contributions of Ca$_v$2.2 currents and Ca^{2+}-independent mechanisms to sustain release during high-frequency synaptic activity.
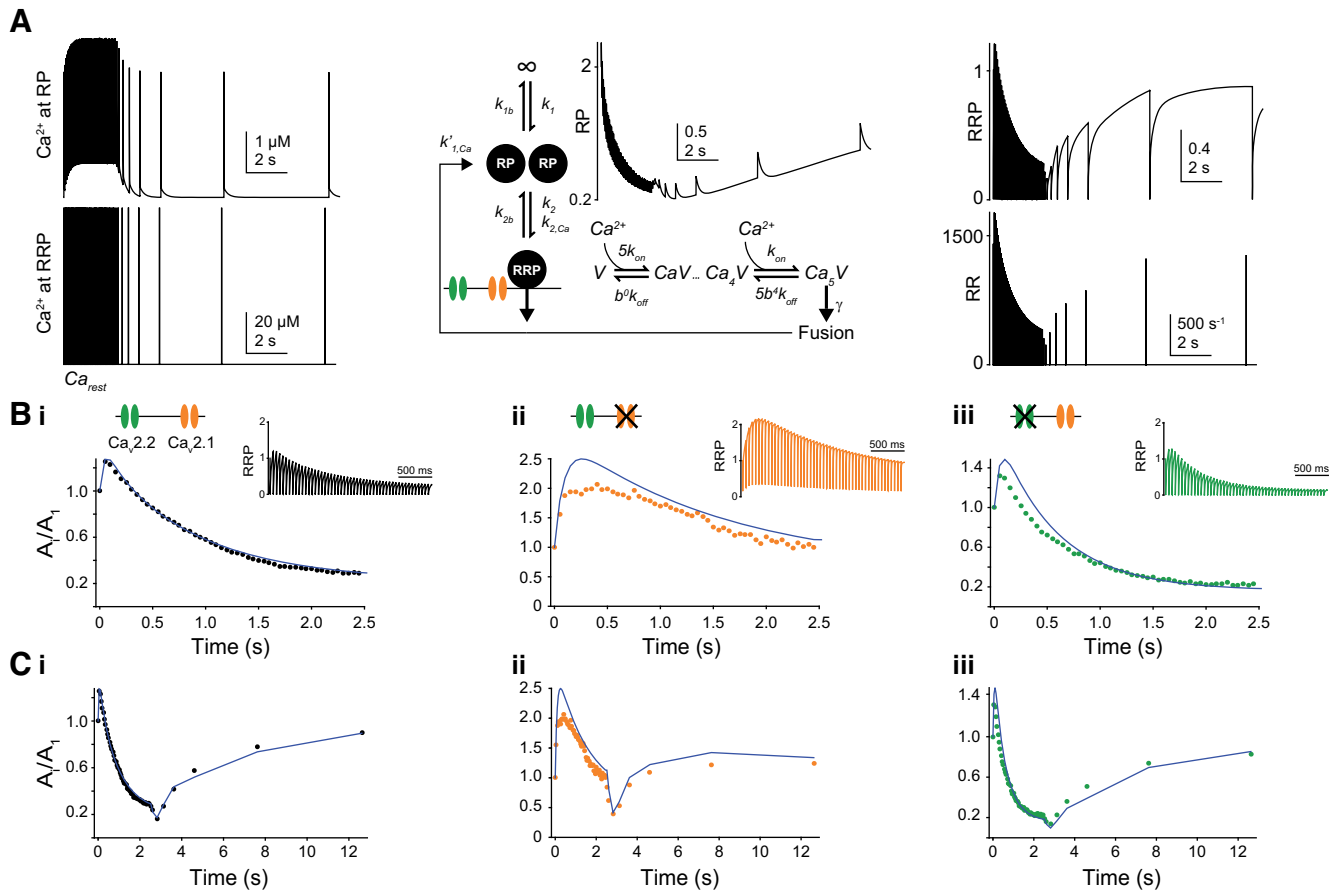
Figure 7. A sequential vesicle pool model with Ca^{2+}-dependent and Ca^{2+}-independent rate constants predicts the experimental data. ***A***, Middle, The model covered a five-site release sensor (RRP, V) with recruitment via an RP that in turn is replenished via an infinite reserve pool and via recycling of fused vesicles. Rate constants of recruitment were Ca^{2+} dependent or Ca^{2+} independent, as indicated. Left, The model was driven by [Ca^{2+}]$_i$ resulting from AP-induced opening of Ca$_v$2.1 (orange) and Ca$_v$2.2 (green) channels. Fifty APs at 20 Hz followed by the recovery train were simulated. Release was triggered by the local [Ca^{2+}]$_i$ at the RRP (bottom), resulting from the opening of 1 tightly coupled Ca$_v$2.1 (distance, 10 nm) and 2 more remote Ca$_v$2.2 (24 nm) channels. Ca^{2+}-dependent recruitment was driven by the global [Ca^{2+}]$_i$ (top) from 6 Ca$_v$2.1 and 2 Ca$_v$2.2 channels. The driving force for Ca^{2+} influx was set according to 6 mm [Ca^{2+}]$_e$. Top middle and right, The graphs show the changes over time in the RP and RRP, and the release rate during the train and the recovery under baseline conditions. RRP during toxin treatment is shown in ***B***. A table with the model parameters is given in Table 1. ***Bi***, Fit of the simulation (blue line) to the average experimental data during the 50 AP train at 20 Hz (black). The rate constants of recruitment were the free parameters during model adjustment. Inset, Simulation of RRP during the 20 Hz train of APs under baseline conditions. Note the initial overfilling of the RRP. ***Bii, iii***, As in ***i*** but for the block of Ca$_v$2.1 (***ii***) or Ca$_v$2.2 (***iii***) channels. All other parameters were kept as in ***i***. The results of the simulations (blue lines) are shown superimposed on the corresponding experimental data (orange or green). Insets, Simulations of RRP. Note the persisting overfilling of the RRP during Ca$_v$2.1 block (***Bii***) and the more rapid decline in the RRP to a lower steady state compared with the baseline conditions due to the block of Ca$_v$2.2 (***Biii***). ***Ci–iii***, As in ***Bi–iii*** but for entire traces including the recovery.

Discussion

The focus of this study was on the function of Ca$_v$2.2 in matured PF boutons. Ca$_v$2.2 and Ca$_v$2.3 lose their function in gating AP-evoked release during the maturation of glutamatergic synapses, such that in mature glutamatergic boutons the release is almost exclusively triggered via Ca$_v$2.1 (Iwasaki and Takahashi, 1998; Iwasaki et al., 2000; Fedchyshyn and Wang, 2005; Miki et al., 2013; Nakamura et al., 2015; Kusch et al., 2018; Bornschein et al., 2019). However, Ca$_v$2.2 and Ca$_v$2.3 remain present in matured PF boutons (Myoga and Regehr, 2011; Baur et al., 2015; Kusch et al., 2018), but the functional significance particularly of Ca$_v$2.2 remained elusive. We found that none of the Ca$_v$2.1 to Ca$_v$2.3 channels were engaged in triggering AP-independent spontaneous release. Yet, our results suggest that Ca$_v$2.2 channels, but not Ca$_v$2.3 channels, significantly boost the recruitment of vesicles to release sites during continuing AP-evoked synaptic transmission.

Release can occur as a spontaneous release of individual quanta (mEPSCs; or "minis") or as an AP-evoked release. The dependency on [Ca^{2+}]$_i$ and the involvement of Ca$_v$s is thought to differ between the two modes of release (Smith et al., 2012;

Schneggenburger and Rosenmund, 2015; Williams and Smith, 2018). Here and in a previous study (Yamasaki et al., 2006), the frequency of cerebellar mEPSCs was found to increase in elevated [Ca^{2+}]$_e$. Similar findings come from several synapses (Williams and Smith, 2018). Potential mechanisms for this effect of [Ca^{2+}]$_e$ include stochastic openings of Ca$_v$2 forming transient presynaptic [Ca^{2+}]$_i$ nanodomains (Ermolyuk et al., 2013) and increases in the presynaptic [Ca^{2+}]$_i$ independent of the opening of Ca$_v$s (Yamasaki et al., 2006). An increase in presynaptic [Ca^{2+}]$_i$ could activate sensors of the Synaptotagmin (Xu et al., 2009) or Doc2 family (Groffen et al., 2010; but see Pang et al., 2011). Alternatively, extracellular Ca^{2+} could activate the G-protein-coupled Ca^{2+}-sensing receptor (Vyleta and Smith, 2011). These potential mechanisms are not mutually exclusive.

In cultured hippocampal neurons, the frequency of mEPSCs was significantly reduced by application of the Ca$_v$2 subtype-specific toxins AgTx, CTx, and SNX (Ermolyuk et al., 2013). In light of this, we examined a possible function of Ca$_v$2 subtypes in gating spontaneous glutamate release by using AgTx, CTx, and SNX in our cerebellar slices. However, our results revealed no susceptibility of cerebellar glutamatergic minis
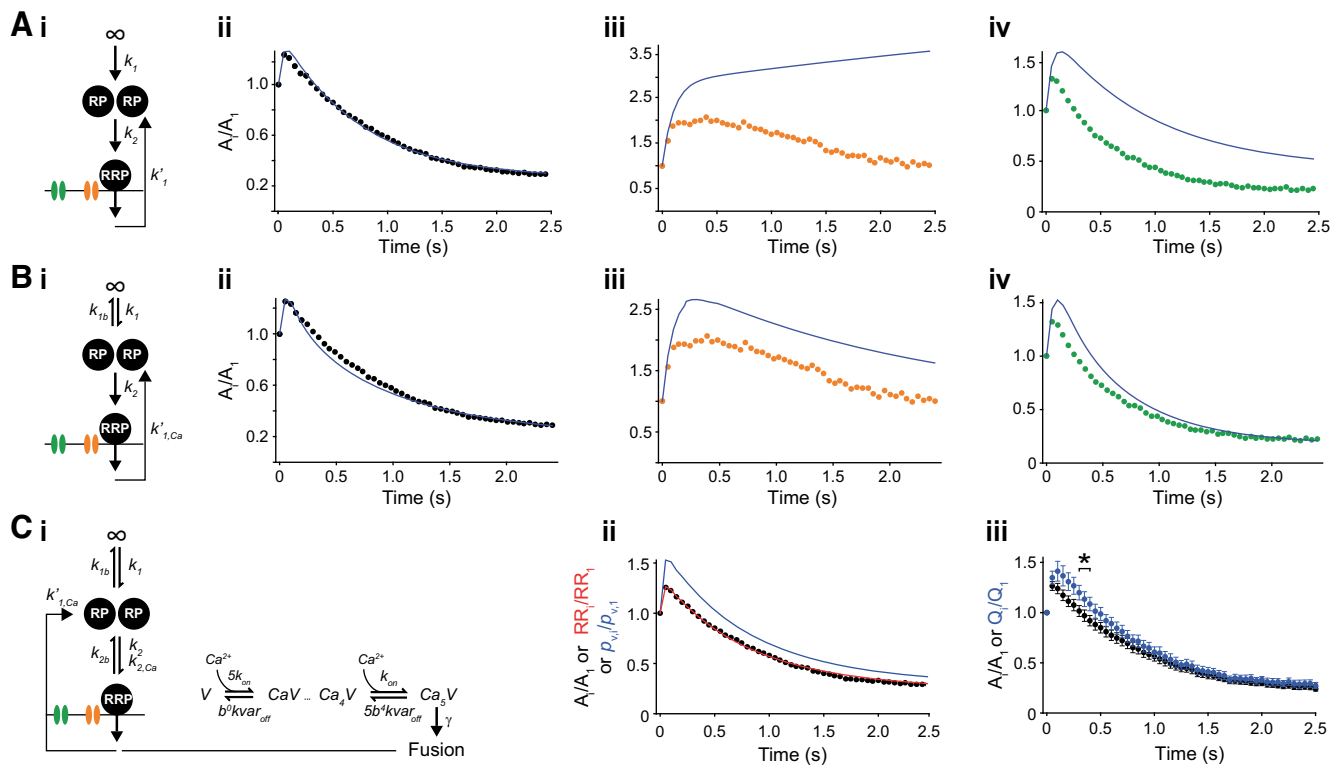
Figure 8. Model development and alternative models. ***Ai***, A simplified version of the sequential model in which all rate constants were Ca^{2+} independent. In this model, 80% of the fused vesicles were recycled into the RP. ***Aii***, The rate constants were adjusted to fit (blue line) the experimental data under baseline conditions during the train (black). ***Aiii, iv***, As in ***ii*** but for block of Ca$_v$2.1 (***iii***, orange) or Ca$_v$2.2 (***iv***, green) channels. Model parameters were kept as in ***ii***. ***Bi–iv***, Same as in ***Ai–iv*** except that k'_1 was Ca^{2+} dependent ($k'_{1,Ca}$) and that all fused vesicles could be recycled. Note that this modification was sufficient to capture the general characteristics of the experimental curves, although the fit to the data with block of Ca$_v$2.1 is still poor. ***Ci***, Alternative model to Figure 7A in which facilitation of the release sensor ($kvar_{off}$) was introduced (for details, see Materials and Methods). ***Cii***, The rate constants were adjusted such that the normalized peak release rates (RR$_i$/RR$_1$; red) fitted the experimental baseline data (black). The blue line shows the normalized p_v (i.e., RR integrated over time and normalized to RR$_1$). Note the deviation between the two simulations, which results from broadening of the RR during the train. ***Ciii***, EPSC amplitudes (A$_i$) normalized to the first amplitude (A$_1$; black) compared with the time-integrated EPSCs (Q$_i$) normalized to Q$_1$ (blue). The deviation between the two curves was slightly significant only for the indicated range (7th EPSC, *p = 0.021; 8th EPSC, *p = 0.031; 9th EPSC, *p = 0.025) but not over the entire time course as predicted in ***Cii***.

to either of the toxins or their combination, despite their dependency on [Ca^{2+}]$_e$ (Fig. 1). This is similar to cultured neocortical neurons, where both Cd^{2+} (Tsintsadze et al., 2017) and MVIIC (Tsintsadze et al., 2017), a peptide toxin specific for Ca$_v$2.1 and Ca$_v$2.2, did not affect spontaneous glutamate release. We conclude from our experiments with Ca$_v$2-specific toxin blockers that the functional significance of Ca$_v$2.2 in matured PF boutons cannot reside in gating spontaneous release.

During high-frequency evoked release in near physiological [Ca^{2+}]$_e$, PF synapses show pronounced and sustained facilitation that relies largely on ultrarapid vesicle recruitment (Valera et al., 2012; Miki et al., 2016; Doussau et al., 2017). Recruitment is considered to be at least partially Ca^{2+} dependent (Brachtendorf et al., 2015; Miki et al., 2016; Doussau et al., 2017; Miki et al., 2018). Here, we probed whether Ca$_v$2.2 and Ca$_v$2.3 are Ca^{2+} sources driving recruitment in matured PF terminals, first using brief bursts of APs and near physiological [Ca^{2+}]$_e$ of 2 mM. Since neither a Ca$_v$2.2 nor a Ca$_v$2.3 blocker affected the first EPSC (Kusch et al., 2018), a reduction in subsequent amplitudes would likely reflect a contribution to recruitment. However, we also found that the successional EPSC amplitudes remained unaffected (Fig. 2), arguing against a substantial contribution of Ca$_v$2.2 and Ca$_v$2.3 to driving ultrafast recruitment during brief bursts of APs.

During sensory stimulation (van Beugen et al., 2013) and locomotion (Powell et al., 2015), granule cells fire high-frequency

bursts consisting of tens of APs *in vivo*. Their PF–PN synapses maintain facilitation for ≥20 APs during high-frequency activation and only thereafter start to depress (Doussau et al., 2017). To test for a contribution of Ca$_v$2.2 and Ca$_v$2.3 to vesicle recruitment during later phases of heavy synaptic use, we investigated 20 Hz trains of 50 APs in elevated [Ca^{2+}]$_e$ of 6 mM. Under these conditions, synapses were driven effectively into the steady state between release and recruitment required for cumulative analysis (Schneggenburger et al., 1999; Neher, 2015), thereby concomitantly avoiding the buildup of a tonic component in the EPSC trains that occurred at higher frequencies even in lower [Ca^{2+}]$_e$ (Doussau et al., 2017). Indeed, we found that blocking Ca$_v$2.2 significantly reduced the steady-state EPSC amplitudes (Fig. 4C). In the cumulative analysis the slope was significantly reduced, while the *y*-intercept remained statistically unaffected by the application of CTx. These results are consistent with Ca$_v$2.2 channels being regulators of the recruitment rate (Fig. 3C,D). In support of this notion, strong block of Ca$_v$2.1 tended to increase release later during the train, while strongly reducing release during its initial phase. In the cumulative analysis, an increased slope and a decreased *y*-intercept resulted (Figs. 4A, 5A). Our models indicate that this results from a combination of the reduced consumption of vesicles from the RRP because of low p_v with the intact recruitment partially via Ca^{2+} influx through Ca$_v$2.2 (Figs. 3, 7). Yet, our data do not allow exclusion of the more complex assumption that there is a difference between vesicles recruited

early or late in the train with regard to their coupling to either Ca$_v$2.1 or Ca$_v$2.2 channels.

Steady-state release late in the train was reduced but not abolished by block of Ca$_v$2.2, which indicated additional sources driving recruitment. Weak block of Ca$_v$2.1 suggested a contribution of these channels to steady-state recruitment (Fig. 4D) that was masked if Ca$_v$2.1 were blocked strongly. Our data indicate that this masking resulted from the absence of a depressed steady state as a result of the lasting overfilling of the RRP during strong block of Ca$_v$2.1 (Fig. 7).

SNX, which specifically, but incompletely, blocks Ca$_v$2.3 (Myoga and Regehr, 2011), did not affect any phase of the train, arguing against a contribution of Ca$_v$2.3 channels to release, recruitment, and short-term facilitation (Fig. 4B). This confirms previous findings about Ca$_v$2.3 channels in release and facilitation (Dietrich et al., 2003; Myoga and Regehr, 2011; Kusch et al., 2018), and extends these findings by showing that SNX-sensitive Ca$_v$2.3 channels are also not involved in steady-state recruitment.

Finally, block of Ca$_v$2.3 or Ca$_v$2.2 did not significantly affect the time course of recovery (Fig. 6). Together with the absence of an effect on EPSC amplitudes during brief bursts (Fig. 2), this indicated the presence of additional basal recruitment. Thus, our results suggest that recruitment in mature PF boutons has a basal component and is boosted by Ca^{2+} influx through Ca$_v$2.2 and Ca$_v$2.1. With respect to the presence of basal and Ca^{2+}-boosted recruitment, PF synapses appear to be similar to other central synapses, although the values of the rate constants may differ substantially and the specific Ca^{2+} sources were not identified at other synapses (Sakaba, 2008; Eshra et al., 2021; Lin et al., 2022).

With respect to the sag, PF synapses might differ from other synapses, similar to their quite specific high-frequency facilitation and low-frequency depression (Doussau et al., 2017). The sag occurred independent of the application of any of the three toxins (Fig. 6). Hence, the mechanisms underlying regulation of the sag are likely to be independent of the Ca^{2+}-dependent processes regulating recruitment. In a recent zap-and-freeze EM study on hippocampal boutons, it was found that following an AP new vesicles rapidly, but transiently, replenished the RRP. The transient docking was followed by stable docking only on a slower timescale (Kusick et al., 2020). Although our experiments do not allow analyzing undocking following a single AP, we consider it possible that the sag in our experiments reflects an increased tendency of rapidly recruited vesicles to leave the RRP. Consistently, a prior study at PF–PN synapses concluded that rapid recruitment is reversible (Doussau et al., 2017).

To summarize, our data agree with an essential determination of p_v by tightly coupled Ca$_v$2.1 in mature PF boutons. They suggest an important regulatory function of more remote Ca$_v$2.2 for sustaining the efficacy of mature PF synaptic transmission during burst of tens of APs.

References

Abenavoli A, Forti L, Bossi M, Bergamaschi A, Villa A, Malgaroli A (2002) Multimodal quantal release at individual hippocampal synapses: evidence for no lateral inhibition. J Neurosci 22:6336–6346.

Allbritton NL, Meyer T, Stryer L (1992) Range of messenger action of calcium ion and inositol 1,4,5-trisphosphate. Science 258:1812–1815.

Arendt O, Schwaller B, Brown EB, Eilers J, Schmidt H (2013) Restricted diffusion of calretinin in cerebellar granule cell dendrites implies Ca^{2+}-dependent interactions via its EF-hand 5 domain. J Physiol 591:3887–3899.

Bastianelli E (2003) Distribution of calcium-binding proteins in the cerebellum. Cerebellum 2:242–262.

Baur D, Bornschein G, Althof D, Watanabe M, Kulik A, Eilers J, Schmidt H (2015) Developmental tightening of cerebellar cortical synaptic influx-release coupling. J Neurosci 35:1858–1871.

Bornschein G, Arendt O, Hallermann S, Brachtendorf S, Eilers J, Schmidt H (2013) Paired-pulse facilitation at recurrent Purkinje neuron synapses is independent of calbindin and parvalbumin during high-frequency activation. J Physiol 591:3355–3370.

Bornschein G, Eilers J, Schmidt H (2019) Neocortical high probability release sites are formed by distinct Ca^{2+} channel-to-release sensor topographies during development. Cell Rep 28:1410–1418. e4.

Borst JG, Sakmann B (1998) Calcium current during a single action potential in a large presynaptic terminal of the rat brainstem. J Physiol 506:143–157.

Brachtendorf S, Eilers J, Schmidt H (2015) A use-dependent increase in release sites drives facilitation at calretinin-deficient cerebellar parallel-fiber synapses. Front Cell Neurosci 9:27.

Brémaud A, West DC, Thomson AM (2007) Binomial parameters differ across neocortical layers and with different classes of connections in adult rat and cat neocortex. Proc Natl Acad Sci U S A 104:14134–14139.

Brenowitz SD, Regehr WG (2007) Reliability and heterogeneity of calcium signaling at single presynaptic boutons of cerebellar granule cells. J Neurosci 27:7888–7898.

Bucurenciu I, Kulik A, Schwaller B, Frotscher M, Jonas P (2008) Nanodomain coupling between Ca^{2+} channels and Ca^{2+} sensors promotes fast and efficient transmitter release at a cortical GABAergic synapse. Neuron 57:536–545.

Bucurenciu I, Bischofberger J, Jonas P (2010) A small number of open Ca^{2+} channels trigger transmitter release at a central GABAergic synapse. Nat Neurosci 13:19–21.

Delvendahl I, Jablonski L, Baade C, Matveev V, Neher E, Hallermann S (2015) Reduced endogenous Ca^{2+} buffering speeds active zone Ca^{2+} signaling. Proc Natl Acad Sci U S A 112:E3075–E3084.

Dietrich D, Kirschstein T, Kukley M, Pereverzev A, von der Brelie C, Schneider T, Beck H (2003) Functional specialization of presynaptic Ca$_v$2.3 Ca^{2+} channels. Neuron 39:483–496.

Doussau F, Schmidt H, Dorgans K, Valera AM, Poulain B, Isope P (2017) Frequency-dependent mobilization of heterogeneous pools of synaptic vesicles shapes presynaptic plasticity. Elife 6:e28935.

Ermolyuk YS, Alder FG, Surges R, Pavlov IY, Timofeeva Y, Kullmann DM, Volynski KE (2013) Differential triggering of spontaneous glutamate release by P/Q-, N- and R-type Ca^{2+} channels. Nat Neurosci 16:1754–1763.

Eshra A, Schmidt H, Eilers J, Hallermann S (2021) Calcium dependence of neurotransmitter release at a high fidelity synapse. Elife 10:e70408.

Faas GC, Schwaller B, Vergara JL, Mody I (2007) Resolving the fast kinetics of cooperative binding: Ca^{2+} buffering by calretinin. PLoS Biol 5:e311.

Fedchyshyn MJ, Wang LY (2005) Developmental transformation of the release modality at the calyx of Held synapse. J Neurosci 25:4131–4140.

Groffen AJ, Martens S, Diez Arazola R, Cornelisse LN, Lozovaya N, de Jong AP, Goriounova NA, Habets RL, Takai Y, Borst JG, Brose N, McMahon HT, Verhage M (2010) Doc2b is a high-affinity Ca^{2+} sensor for spontaneous neurotransmitter release. Science 327:1614–1618.

Imig C, López-Murcia FJ, Maus L, García-Plaza IH, Mortensen LS, Schwark M, Schwarze V, Angibaud J, Nägerl UV, Taschenberger H, Brose N, Cooper BH (2020) Ultrastructural imaging of activity-dependent synaptic membrane-trafficking events in cultured brain slices. Neuron 108:843–860.e8.

Iwasaki S, Takahashi T (1998) Developmental changes in calcium channel types mediating synaptic transmission in rat auditory brainstem. J Physiol 509:419–423.

Iwasaki S, Momiyama A, Uchitel OD, Takahashi T (2000) Developmental changes in calcium channel types mediating central synaptic transmission. J Neurosci 20:59–65.

Katz B, Miledi R (1968) The role of calcium in neuromuscular facilitation. J Physiol 195:481–492.

Kusch V, Bornschein G, Loreth D, Bank J, Jordan J, Baur D, Watanabe M, Kulik A, Heckmann M, Eilers J, Schmidt H (2018) Munc13-3 is required for the developmental localization of Ca^{2+} channels to active zones and the nanopositioning of Ca$_v$2.1 near release sensors. Cell Rep 22:1965–1973.

Kusick GF, Chin M, Raychaudhuri S, Lippmann K, Adula KP, Hujber EJ, Vu T, Davis MW, Jorgensen EM, Watanabe S (2020) Synaptic vesicles transiently dock to refill release sites. Nat Neurosci 23:1329–1338.

Li L, Bischofberger J, Jonas P (2007) Differential gating and recruitment of P/Q-, N-, and R-type Ca^{2+} channels in hippocampal mossy fiber boutons. J Neurosci 27:13420–13429.

Lin K-H, Taschenberger H, Neher E (2022) A sequential two-step priming scheme reproduces diversity in synaptic strength and short-term plasticity. Proc Natl Acad Sci U S A 119:e2207987119.

Meinrenken CJ, Borst JG, Sakmann B (2002) Calcium secretion coupling at calyx of held governed by nonuniform channel-vesicle topography. J Neurosci 22:1648–1667.

Miki T, Hirai H, Takahashi T (2013) Activity-dependent neurotrophin signaling underlies developmental switch of Ca^{2+} channel subtypes mediating neurotransmitter release. J Neurosci 33:18755–18763.

Miki T, Malagon G, Pulido C, Llano I, Neher E, Marty A (2016) Actin- and myosin-dependent vesicle loading of presynaptic docking sites prior to exocytosis. Neuron 91:808–823.

Miki T, Nakamura Y, Malagon G, Neher E, Marty A (2018) Two-component latency distributions indicate two-step vesicular release at simple glutamatergic synapses. Nat Commun 9:3943.

Miki T, Midorikawa M, Sakaba T (2020) Direct imaging of rapid tethering of synaptic vesicles accompanying exocytosis at a fast central synapse. Proc Natl Acad Sci U S A 117:14493–14502.

Millar AG, Zucker RS, Ellis-Davies GC, Charlton MP, Atwood HL (2005) Calcium sensitivity of neurotransmitter release differs at phasic and tonic synapses. J Neurosci 25:3113–3125.

Mintz IM, Sabatini BL, Regehr WG (1995) Calcium control of transmitter release at a cerebellar synapse. Neuron 15:675–688.

Myoga MH, Regehr WG (2011) Calcium microdomains near R-type calcium channels control the induction of presynaptic long-term potentiation at parallel fiber to Purkinje cell synapses. J Neurosci 31:5235–5243.

Nakamura Y, Harada H, Kamasawa N, Matsui K, Rothman JS, Shigemoto R, Silver RA, DiGregorio DA, Takahashi T (2015) Nanoscale distribution of presynaptic Ca^{2+} channels and its impact on vesicular release during development. Neuron 85:145–158.

Neher E (2015) Merits and limitations of vesicle pool models in view of heterogeneous populations of synaptic vesicles. Neuron 87:1131–1142.

Neher E, Brose N (2018) Dynamically primed synaptic vesicle states: key to understand synaptic short-term plasticity. Neuron 100:1283–1291.

Neher E, Sakaba T (2008) Multiple roles of calcium ions in the regulation of neurotransmitter release. Neuron 59:861–872.

Newcomb R, Szoke B, Palma A, Wang G, Chen X, Hopkins W, Cong R, Miller J, Urge L, Tarczy-Hornoch K, Loo JA, Dooley DJ, Nadasdi L, Tsien RW, Lemos J, Miljanich G (1998) Selective peptide antagonist of the class E calcium channel from the venom of the tarantula Hysterocrates gigas. Biochemistry 37:15353–15362.

Palay SL, Chan-Palay V (1974) Cerebellar cortex: cytology and organization. Berlin: Springer.

Pang ZP, Bacaj T, Yang X, Zhou P, Xu W, Südhof TC (2011) Doc2 supports spontaneous synaptic transmission by a Ca^{2+}-independent mechanism. Neuron 70:244–251.

Powell K, Mathy A, Duguid I, Häusser M (2015) Synaptic representation of locomotion in single cerebellar granule cells. Elife 4:e07290.

Rothman JS, Silver RA (2018) NeuroMatic: an integrated open-source software toolkit for acquisition, analysis and simulation of electrophysiological data. Front Neuroinform 12:14.

Sabatini BL, Regehr WG (1998) Optical measurement of presynaptic calcium currents. Biophys J 74:1549–1563.

Sakaba T (2008) Two Ca^{2+}-dependent steps controlling synaptic vesicle fusion and replenishment at the cerebellar basket cell terminal. Neuron 57:406–419.

Schiffmann SN, Cheron G, Lohof A, D'Alcantara P, Meyer M, Parmentier M, Schurmans S (1999) Impaired motor coordination and Purkinje cell excitability in mice lacking calretinin. Proc Natl Acad Sci U S A 96:5257–5262.

Schmidt H (2019) Control of presynaptic parallel fiber efficacy by activity-dependent regulation of the number of occupied release sites. Front Syst Neurosci 13:30.

Schmidt H, Schwaller B, Eilers J (2005) Calbindin D28k targets myo-inositol monophosphatase in spines and dendrites of cerebellar Purkinje neurons. Proc Natl Acad Sci U S A 102:5850–5855.

Schmidt H, Stiefel K, Racay P, Schwaller B, Eilers J (2003) Mutational analysis of dendritic Ca^{2+} kinetics in rodent Purkinje cells: role of parvalbumin and calbindin D$_{28k}$. J Physiol 551:13–32.

Schmidt H, Brachtendorf S, Arendt O, Hallermann S, Ishiyama S, Bornschein G, Gall D, Schiffmann SN, Heckmann M, Eilers J (2013) Nanodomain coupling at an excitatory cortical synapse. Curr Biol 23:244–249.

Schneggenburger R, Meyer AC, Neher E (1999) Released fraction and total size of a pool of immediately available transmitter quanta at a calyx synapse. Neuron 23:399–409.

Schneggenburger R, Rosenmund C (2015) Molecular mechanisms governing Ca^{2+} regulation of evoked and spontaneous release. Nat Neurosci 18:935–941.

Scimemi A, Diamond JS (2012) The number and organization of Ca^{2+} channels in the active zone shapes neurotransmitter release from Schaffer collateral synapses. J Neurosci 32:18157–18176.

Scott R, Rusakov DA (2006) Main determinants of presynaptic Ca^{2+} dynamics at individual mossy fiber-CA3 pyramidal cell synapses. J Neurosci 26:7071–7081.

Silva M, Tran V, Marty A (2021) Calcium-dependent docking of synaptic vesicles. Trends Neurosci 44:579–592.

Smith SM, Chen W, Vyleta NP, Williams C, Lee CH, Phillips C, Andresen MC (2012) Calcium regulation of spontaneous and asynchronous neurotransmitter release. Cell Calcium 52:226–233.

Tsintsadze T, Williams CL, Weingarten DJ, von Gersdorff H, Smith SM (2017) Distinct actions of voltage-activated Ca^{2+} channel block on spontaneous release at excitatory and inhibitory central synapses. J Neurosci 37:4301–4310.

Valera AM, Doussau F, Poulain B, Barbour B, Isope P (2012) Adaptation of granule cell to Purkinje cell synapses to high-frequency transmission. J Neurosci 32:3267–3280.

van Beugen BJ, Gao Z, Boele H-J, Hoebeek F, de Zeeuw CI (2013) High frequency burst firing of granule cells ensures transmission at the parallel fiber to Purkinje cell synapse at the cost of temporal coding. Front Neural Circuits 7:95.

Vandael D, Borges-Merjane C, Zhang X, Jonas P (2020) Short-term plasticity at hippocampal mossy fiber synapses is induced by natural activity patterns and associated with vesicle pool engram formation. Neuron 107:509–521.e7.

Vyleta NP, Jonas P (2014) Loose coupling between Ca^{2+} channels and release sensors at a plastic hippocampal synapse. Science 343:665–670.

Vyleta NP, Smith SM (2011) Spontaneous glutamate release is independent of calcium influx and tonically activated by the calcium-sensing receptor. J Neurosci 31:4593–4606.

Williams CL, Smith SM (2018) Calcium dependence of spontaneous neurotransmitter release. J Neurosci Res 96:335–347.

Winsky L, Kuźnicki J (1995) Distribution of calretinin, calbindin D28k, and parvalbumin in subcellular fractions of rat cerebellum: effects of calcium. J Neurochem 65:381–388.

Xu J, Pang ZP, Shin OH, Südhof TC (2009) Synaptotagmin-1 functions as a Ca^{2+} sensor for spontaneous release. Nat Neurosci 12:759–766.

Yamasaki M, Hashimoto K, Kano M (2006) Miniature synaptic events elicited by presynaptic Ca^{2+} rise are selectively suppressed by cannabinoid receptor activation in cerebellar Purkinje cells. J Neurosci 26:86–95.